AD-A111 168 AIR FORCE INST OF TECH WRIGHT-PATTERSON AFB OH SCHOO--ETC F/G 20/4
INVESTIGATION OF UPWIND SCHEMES FOR FINITE ELEMENT ANALYSIS OF --ETC(U)
DEC 81 D L HUNT
UNCLASSIFIED AFIT/GAE/AA/81D-15 NL

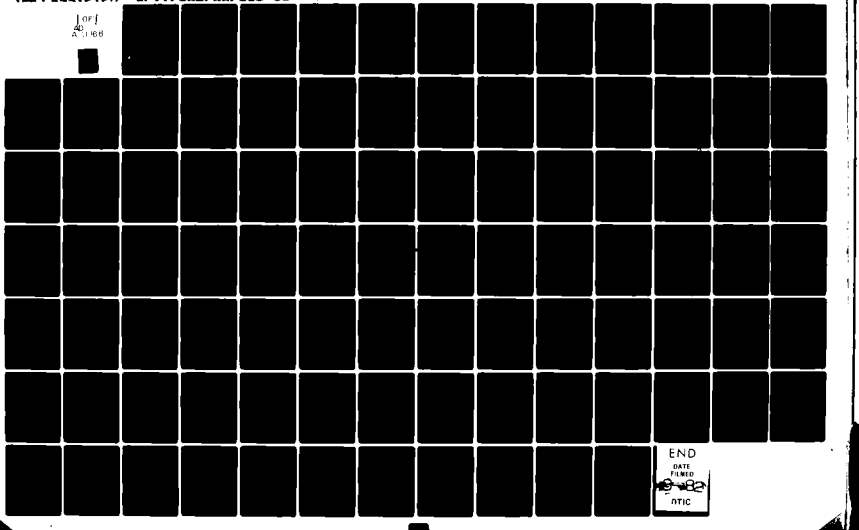

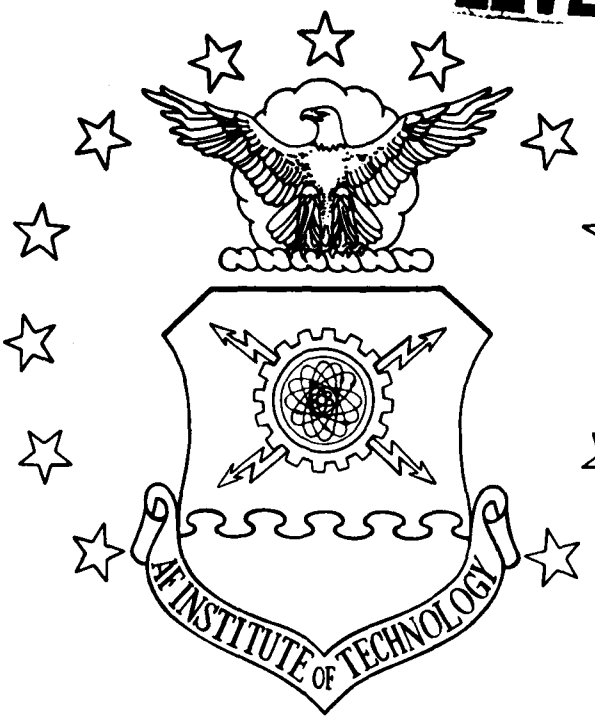

DEPARTMENT OF THE AIR FORCE
AIR UNIVERSITY (ATC)

AIR FORCE INSTITUTE OF TECHNOLOGY

Wright-Patterson Air Force Base, Ohio

AFIT/GAE/AA/81D-15

INVESTIGATION OF UPWIND SCHEMES FOR FINITE ELEMENT ANALYSIS OF TRANSONIC FLOW OVER THIN AIRFOILS

THESIS

AFIT/GAE/AA/81D-15 DENNIS L. HUNT
2d LT USAF

AFIT/GAE/AA/81D-15

INVESTIGATION OF UPWIND SCHEMES FOR FINITE ELEMENT ANALYSIS OF TRANSONIC FLOW OVER THIN AIRFOILS

THESIS

Presented to the Faculty of the School of Engineering
of the Air Force Institute of Technology
Air University
in Partial Fulfillment of the
Requirements for the Degree of
Master of Science

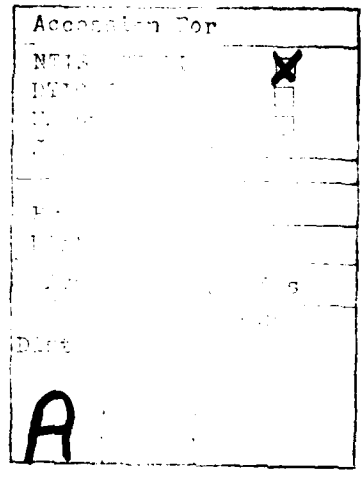

by

Dennis L. Hunt, B.S.A.E.
2nd Lt USAF
Graduate Aeronautical Engineering

December 1981

Approved for public release; distribution unlimited

Preface

I chose this topic because I am interested in fluid flow, but my main field of study at AFIT was structures. Solving a fluid flow problem using a structural method satisfied the requirements of both the school and myself. I would like to thank my advisor Capt J.E. Marsh and my typist Pat Sawdy who patiently helped me to finish this thesis.

Dennis L. Hunt

Contents

Contents (Cont'd)

List of Figures

List of Figures (cont'd)

Abstract

The finite element method was used to solve the two-dimensional, non-linear, small-disturbance, velocity-potential equation for steady transonic flow over a thin airfoil. Two finite element upwind techniques were investigated to see if either could accurately model the supersonic (hyperbolic) zone that is embedded in the subsonic flow field. The two techniques are: upwind functions and an alternative integration scheme. Both techniques used Galerkin's Method of Weighted Residuals, but differed in the supersonic region.

The upwind method involves adding an upwind function to the weight function in order to weight the upstream nodes of an element more than the downstream nodes. The alternative integration method involves Galerkin's method for all elements. In the hyperbolic region, the elemental stiffness matrix is integrated only over the area inside the forward mach cones of the elemental nodes. Both these methods account for the physics involved in supersonic flow. That is, the solution at a point in supersonic flow can only be influenced by points inside the forward mach cone whose apex is located at that point.

Neither of these methods produced results that agree with experimental data or other solutions. The alternative integration method never converged. The upwind method converged, but did not converge to an acceptable solution.

INVESTIGATION OF UPWIND SCHEMES FOR FINITE ELEMENT ANALYSIS OF TRANSONIC FLOW OVER THIN AIRFOILS

I. Introduction

In transonic flow, nonlinear equations with changing characteristics pose major problems in solving the governing equations. These equations need to be solved since many of today's high performance aircraft encounter some form of transonic flow. Over the last fifteen years, investigators have published many papers in this area.

Transonic flow calculations are important, because in this region, violent oscillatory motion is often encountered. If the effects of transonic flow are not incorporated into an aircraft's design, the results could be detrimental to its mission. Whether it be an F-16 going from subsonic to supersonic flight, or the tip of a helicopter blade, the need for transonic flow calculations are evident in today's high technology aircraft.

Most of the work done in transonic flow involves the use of potential flow theory and finite difference methods. The velocity potential equation is used, because for steady, irrotational, frictionless, isentropic flow of a perfect gas, it is a single equation which satisfies the law of conservation of mass, Newton's second principle of motion, and the laws of thermodynamics. Finite difference methods are used, because they have been around for a long time, and have proved

to be a realistic way to solve fluid flow problems. Only recently has the finite element method (FEM) been employed to solve these types of problems. Initially, a method used for structural problems, the FEM is now being investigated to see how well it solves fluid flow problems.

Finite Element Background/Previous Work

The finite element method (FEM) is a numerical method used to solve partial differential equations, and has been around for about thirty years. Prior to the mid 1960's, the FEM was used to solve for static forces in structures. The method was used, because structures are nothing more than an assemblage of finite parts connected at a finite number of points or nodes. Then, forcing equilibrium was enough to determine the loading at each node.

When the mid 1960's came, the FEM had already proved itself useful in solving structural problems using energy principles like the Rayliegh-Ritz method, and was now introduced to non-structural problems such as fluid flow. This worked out very well for simple problems in subsonic flow, and slowly has been proved useful in more complicated non-linear problems such as transonic flow. Now, the FEM is used to solve many types of boundary and initial value problems.

Mathematicians have linked the FEM closely with variational energy concepts with are found in many fields of structures. Since variational principles cannot be found for every problem, the weighted residual method can be used.

This scheme uses such methods as collocation, least squares, and Galerkin's. In this study, Galerkin's Method of Weighted Residuals will be used for the analysis.

Previous work in solving field problems using the FEM goes back to 1965 when Zienkiewiez (Ref 1) published a paper on how to solve Laplace and Poisson equations. A few years later, incompressible flow problems were solved using variational methods and produced encouraging results. For transonic flow, the non-linearity of the equations caused convergence problems in an iterative solution scheme. It was not until 1975, when Shen and Habashi (Ref 2) were able to get converged solutions for mach numbers near critical. Since then, others have obtained converged solutions for transonic flow using different methods. Wellford and Hafez (Refs 3 and 4) used Galerkin's method with iterative solution algorithms based on a velocity approximation. They were able to show convergence properties for freestream mach numbers well into the transonic range. Chan and Brashears (Ref 5) used the least squares method of weighted residuals to obtain solutions for steady and unsteady transonic flow. More recently, Marsh (Ref 6) used a relaxation technique applied to the iterative non-linear term to get converged solutions.

Objective

In this study, the small-disturbance potential equation will be solved using two finite element techniques to see if converged solutions can be obtained in transonic flow over a thin airfoil. The two techniques to be investigated

are an upwind method used by Christie (Ref 7) and Heinrich (Ref 8), and an alternative integration method suggested by J. Marsh. Neither of these methods have been tried in conjunction with transonic potential flow.

The upwind method involves developing upwind functions that when added to the weight functions give the upstream nodes in the supersonic region more influence than the downstream nodes. This is done to account for the fact that in the supersonic region, solutions at the downstream nodes of an element cannot influence solutions at the upstream nodes. In other words, the upwind function should negate the influence of the downstream nodes of an element in the supersonic region.

The alternative integration method involves more of a physically intuitive approach to account for the area that influences the solution at a node in the supersonic part of the flow. Knowing that only the area inside a forward mach cone can influence the nodal parameter, the finite element equations were integrated only over that cone, and not over the entire element as done conventionally in the finite element method.

II. Problem Description

In this study, transonic flow around a thin symmetric non-lifting airfoil will be determined, using potential-flow theory. Solving the steady form of the non-linear small-disturbance potential equation using finite element methods creates a few problems. First, the infinite flow field must be reduced to a finite one so it can be discretized into elements. Second, the governing equation changes character from elliptic to hyperbolic as the flow changes from subsonic to supersonic, and third, the equation is non-linear.

Flow Field

Consider a thin airfoil in an infinite domain Ω with coordinates (x,y) set up so that the origin is at the mid-chord (Fig 1). The freestream is steady uniform flow in the x-direction. The domain Ω extends from the airfoil boundary $\partial\Omega_\alpha$ to infinity as shown in Figure 1.

In order to simplify the problem, a few assumptions are made. The infinite domain will be replaced by a finite one with the boundary $\partial\Omega_\infty + \partial\Omega_\alpha + \partial\Omega_{|x|\geq c/2}$. The airfoil is chosen to be thin, symmetric, parabolic and non-lifting. Thin, so only small perturbation velocities are present. Non-lifting, so that circulation and the Kutta condition do not enter the problem, and symmetric, so that the problem can be formulated in the half space. The new finite domain Ω is shown in Figure 2, and the airfoil planform is given by

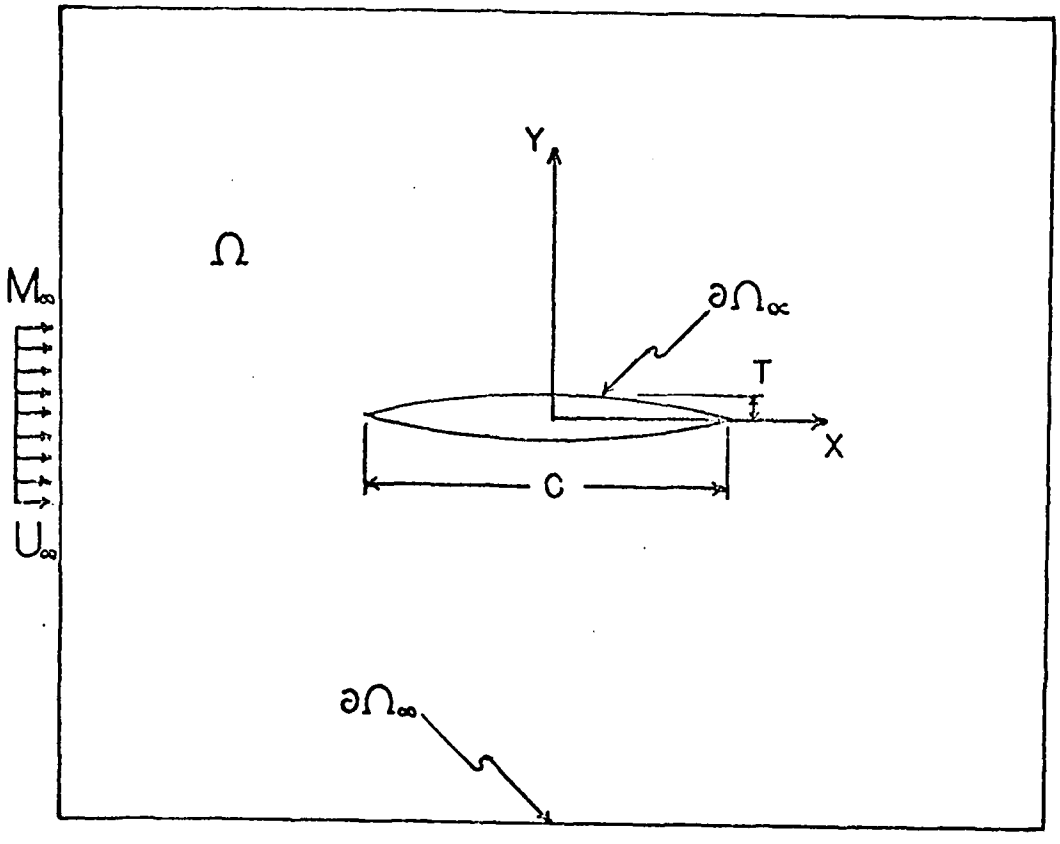

Figure 1. Thin Airfoil in Infinite Steady Freestream

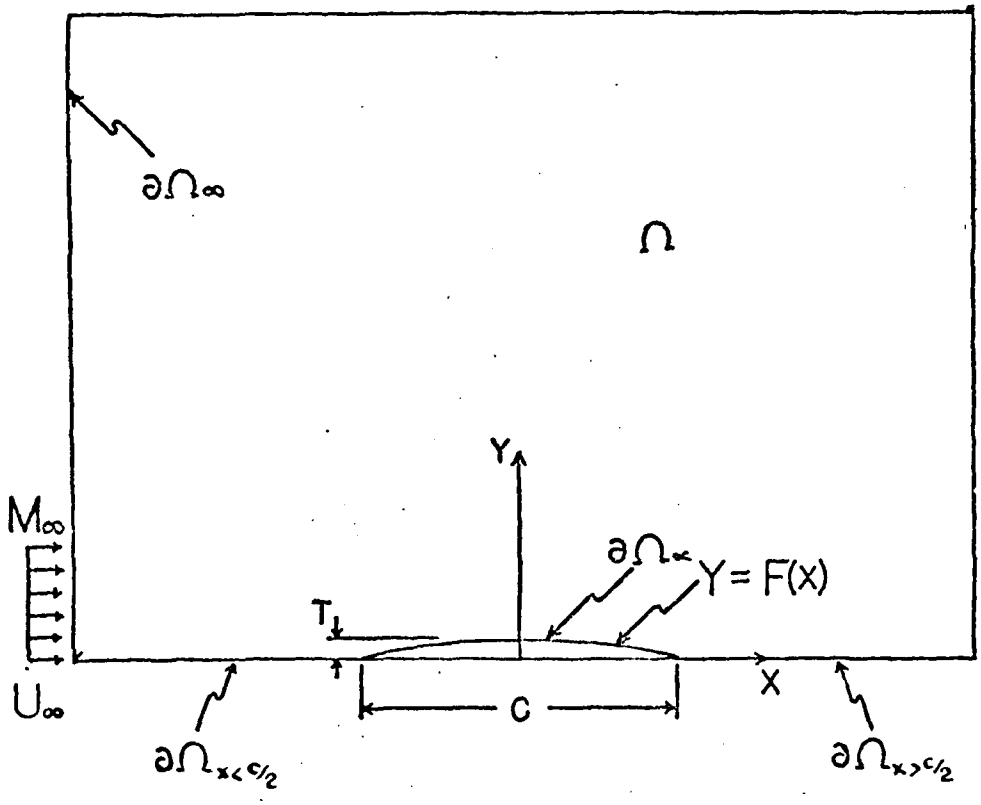

Figure 2. Thin Airfoil in Half Space

$$Y = f(X) = \tau(1 - 4X^2) \qquad (1)$$

where τ is the thickness ratio t/c shown is Figure 2.

Governing Differential Equation

Assuming steady, irrotational, inviscid, isentropic flow of a perfect gas permits the use of potential theory to describe the velocity changes in the freestream. The presence of a thin airfoil permits the use of small-disturbance theory. The non-dimensional small-disturbance potential equation (Ref 9) in terms of the non-dimensional velocity potential is

$$1 - M_\infty^2 - M_\infty^2(1+\gamma)\phi_{,x}\phi_{,xx} + \phi_{,yy} = 0 \qquad (2)$$

where M_∞ is the freestream mach number and γ is the ratio of specific heats (γ=1.4 for air). Equation 2 is valid for all points (x,y) in Ω.

Equation 2 is used for the case of transonic flow where the non-linear term $\phi_{,x}\,\phi_{,xx}$ becomes significant and is required to describe the flow phenomena that occurs. For low mach numbers (i.e. M_∞<0.5) this term is small compared to the others and is often neglected. For the incompressible case (M_∞=0.0) equation 2 reduces to the Laplace equation. In this study, the form of equation 2 will be used for all mach numbers from zero to just less than one.

From partial differential equation theory (Ref 10), eq 2 is referred to as a second-order, non-linear partial

differential equation of mixed character. The equation is second-order, because its highest derivative is a second derivative. Non-linear, because of the $\phi_{,x}\,\phi_{,xx}$ term, and mixed, because the equation changes character from elliptic to hyperbolic as the local velocity goes from subsonic to supersonic, respectively. It is this change, that constitutes the name transonic. This change happens at some critical value of freestream mach number M_{cr} when the flow at a point near the center of the airfoil becomes sonic. As M_∞ is increased further, a region of supersonic flow forms over the airfoil and is called a supersonic bubble. When this region gets big enough, a weak compression shock forms in the downstream part of the bubble to allow the flow to return to subsonic speed. Along the upstream boundary of the supersonic bubble the local mach number is equal to one and the coefficient of the $\phi_{,xx}$ term in eq 2 is zero; therefore, the equation is parabolic. The development for transonic flow over an airfoil is shown in Figure 3.

Boundary Conditions

The boundary conditions for the flow field come from the fact that the perturbation velocities (u,v) must go to zero at infinity, and there cannot be any flow through the boundary of the airfoil $\partial\Omega_\alpha$. In equation form, the boundary conditions are

$$\begin{aligned} &1)\quad \nabla\phi \longrightarrow 0 \quad \text{AS} \quad r \longrightarrow \infty \\ &2)\quad \nabla\vec{\Phi}\cdot\vec{n} = 0 \quad \text{FOR} \quad (X,Y) \ \text{IN} \ \partial\Omega_\alpha \end{aligned} \tag{3}$$

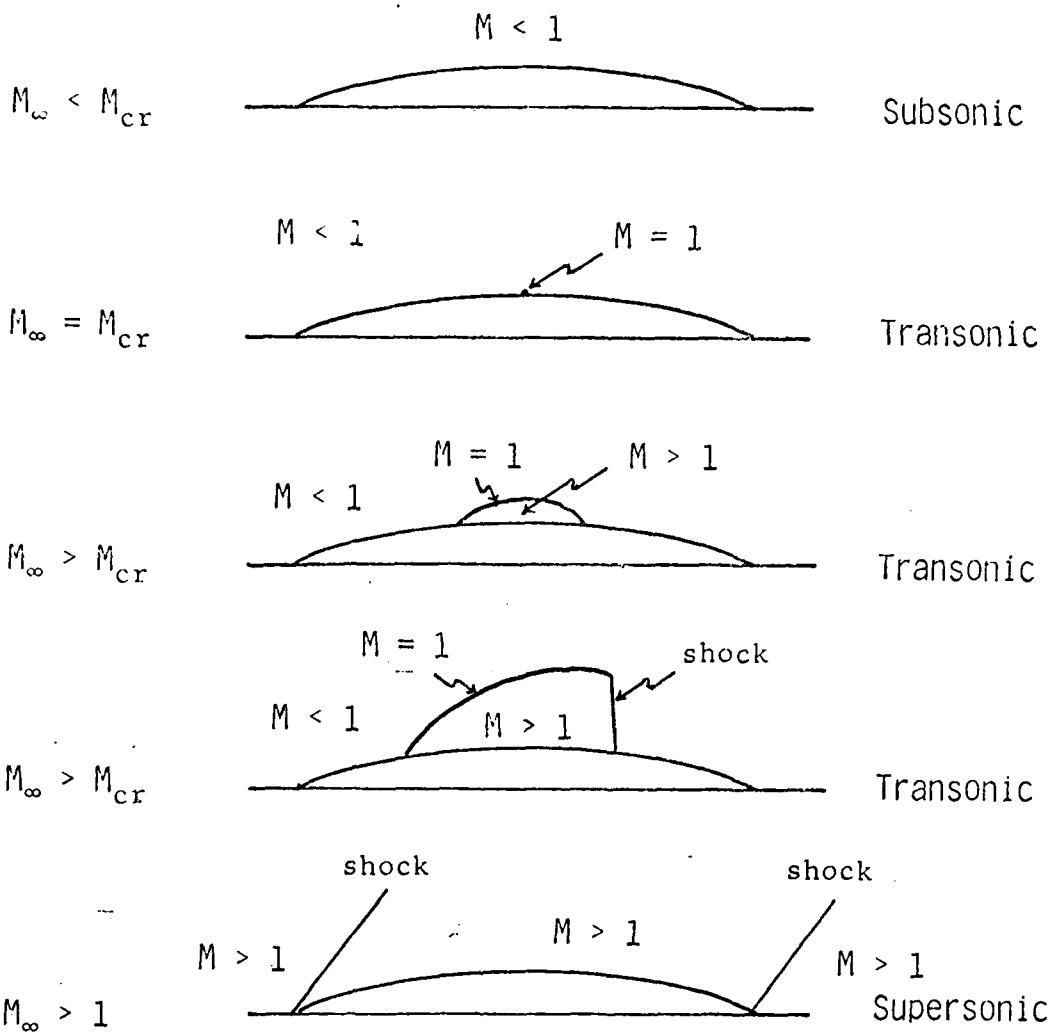

Figure 3. Effect of Freestream Mach Number on Local Mach Number for Thin Airfoils

where r is any distance from the origin, Φ is the full potential and $\vec{n}$ is a unit vector normal to the surface of the airfoil. Further development of these boundary conditions is given in Section III. Along the far field boundary an asymptotic solution developed by Klunker (Ref 11) will be imposed.

III. Analysis

In Section II, the governing equation, the boundary conditions and the difficulties associated with transonic flow calculations were discussed. This chapter describes the formulation techniques necessary to solve the problem numerically using the finite element method. The reader is urged to refer to the appendices for additional information.

Flow Field Discretization

The infinite domain Ω discussed in Section II must be replaced by a finite flow field so that it can be discretized into a finite number of elements. This can be done two ways. First, the far field boundary Ω_f could be taken to be very large, and the actual boundary condition, given by eq 3, be imposed. This choice may not be a good one, because a large flow field requires a greater number of elements, which means higher computational costs. Also, because the boundary conditions are of the Neumann type, the solution can only be determined to within an arbitrary constant unless a specific value of ϕ is given for some arbitrary point (Ref 6).

An alternative technique, used in this study, is to use the far field solution developed by Klunker (Ref 10). For this technique, $\phi = \phi_{FF}$ is specified along the far field boundary. Klunker's solution satisfies the actual boundary condition (eq 3) and is valid only at points in the far field of Ω. This approach has been successfully used by researchers using either finite difference or finite element

(Refs 2,5,6) methods. Klunker's method allows the use of a much smaller domain, as compared to the first method discussed. This small domain means fewer degrees-of-freedom and lower computer costs. Klunker's equation for the far field potential ϕ_{FF} for a non-lifting airfoil, ignoring higher order terms is

$$\phi_{FF} = \frac{1}{\pi\beta} \cdot \frac{X}{X^2+(\beta Y)^2} \int_C f(\xi)\, d\xi \qquad (4)$$

where

$$\beta = \sqrt{1-M_\infty^2}$$

and f(x) is given by eq 1. Evaluating the integral gives

$$\phi_{FF} = \frac{2}{3} \cdot \frac{X\tau}{\pi\beta} \cdot \frac{1}{X^2 + Y^2(1-M_\infty^2)} \qquad (5)$$

which is a function of the location of the far field points.

Working with a symmetric airfoil at zero angle of attack allows the problem to be set up in the half space. The flow field can be designated by two parameters, Xmax and Ymax, as shown in Figure 4. In order to find optimum values for Xmax and Ymax, results of tests done by Marsh (Ref 6) will be used. Marsh, solving this same problem by a different technique, varied the number of elements in the mesh keeping the element size the same. He found that the pressure distribution converged to the assumed solution, for mach numbers from 0.0 to 0.8, when the value for Xmax and Ymax were 1.5 chord lengths or greater. In this study, the minimum dimension (1.5c) will be used for both Xmax and Ymax.

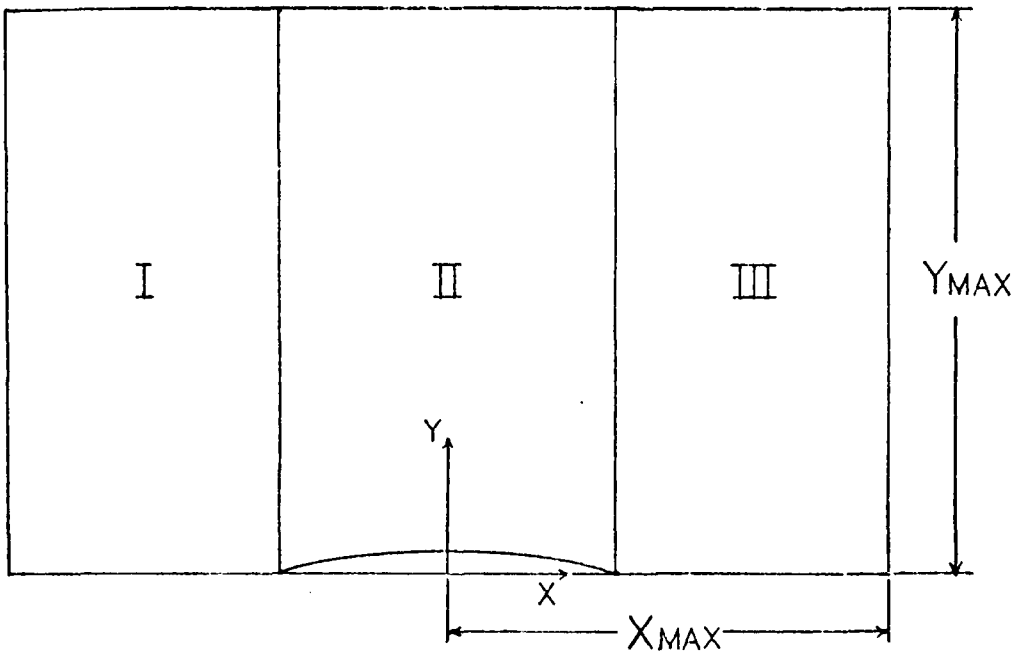

Figure 4. Flow Field Parameters

Working in the half space, the domain of the problem can be broken down into three regions as shown in Figure 4. Regions I and III are upwind and downwind of the airfoil respectively and can be discretized into fairly large elements. Region II, over the airfoil will be discretized finer, because it is here that perturbation velocities change the most. Over the airfoil is also where the pressure distribution is required, so more nodes are needed to accurately depict the pressure distribution. Using a thin airfoil, the boundary terms of the finite element equations (given later in this section) are evaluated along the chord (y=0) of the airfoil. Therefore, the elements in Region II extend down to the x-axis and do not terminate at the airfoil contour.

The mesh shown in Figure 5 is representative of the meshes used in this study. Variations include changing the number of elements over the airfoil, and in Regions I and III.

Finite Element Solution

When solving partial differential equations using finite element methods, it is common practice to transform the governing equation into the form of the matrix equation

$$[K]\{\phi\}=\{F\} \tag{6}$$

where $[K]$ is the stiffness matrix, $\{\phi\}$ is the solution vector and $\{F\}$ is the forcing term. The method of weighted residuals will be used to accomplish this.

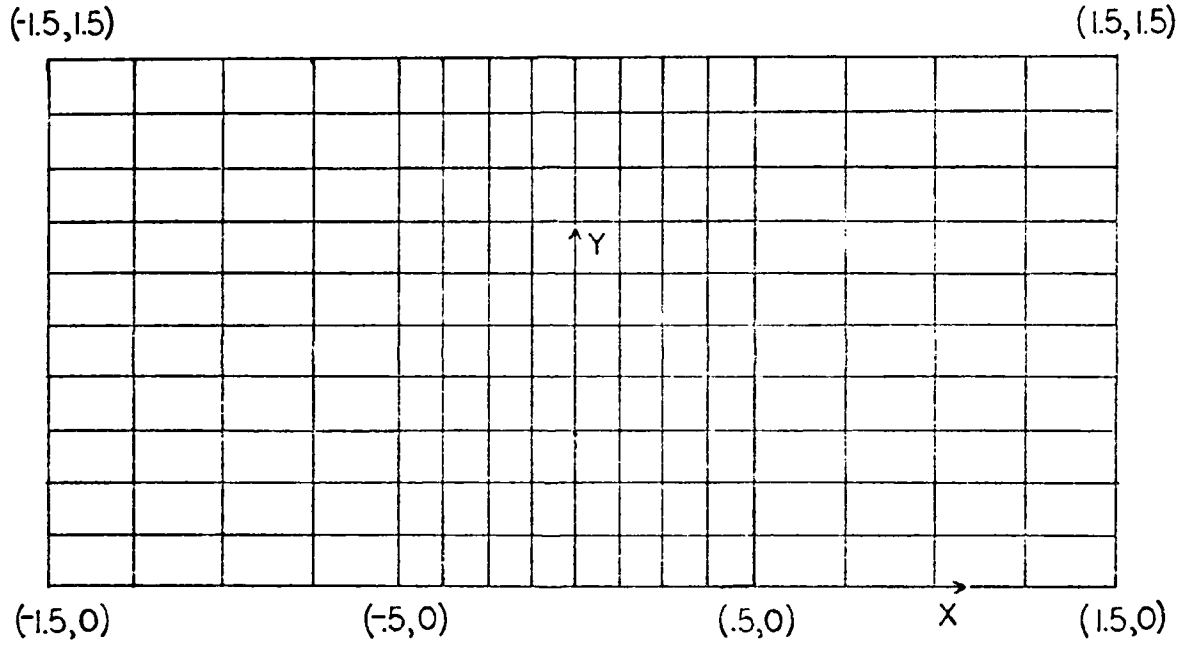

Figure 5. Flow Field Descritization (Grid A)

The steady form of the non-dimensional small-distrubance potential equation (Ref 9) for transonic flow, given by eq 2, in two dimensions is

$$1-M_\infty^2-M_\infty^2(1+\gamma)\,\phi_{,x}\phi_{,xx}+\phi_{,yy}=0 \qquad (2)$$

for all points (x,y) in the domain Ω. Relationships between the non-dimensional parameters (ϕ,x,y) and the physical ones ($\bar{\phi}$,$\bar{x}$,$\bar{y}$) are: $x = \bar{x}/c$, $y = \bar{y}/c$, and $\phi = \bar{\phi}/u_\infty c$, where u_∞ is the freestream velocity and c is the chord length. If eq 2 is formulated by finite element methods, a set of second-order, non-linear algebraic equations will result. This can be simplified two ways, one using an iterative scheme to linearize the non-linear term; and two, integrating by parts to lower the number of continuous derivatives required in the assumed solution so linear elements can be used. Both of these simplifications will be employed in this study, and are elaborated on in the next few paragraphs.

Rewriting eq 2 as

$$\left[(1-M_\infty^2)\phi_{,x}-M_\infty^2(1+\gamma)/2\;\phi_{,x}^2\right]_{,x}+\phi_{,yy}=0 \qquad (7)$$

leaves $\phi_{,x}{}^2$ as the non-linear term. Using the iterative approximation (Ref 6)

$$\phi_{,x}^2 = \phi_{,x}^n\,\phi_{,x}^{n+1} \qquad (8)$$

where superscript n denotes the iteration, allows the potential ϕ to be replaced by a sequence of potentials $\{\phi^0,\phi^1,\ldots,\phi^n,\phi^{n+1}\}$, which converge when

$$\left| \frac{\phi^{n+1} - \phi^{n}}{\phi^{n+1}} \right| \leq \varepsilon^{0} \tag{9}$$

where ε^0 is some small error chosen as the convergence requirement. In this study, ε^0 is chosen to be five hundredths of a percent (Ref 6). Now, eq 7 in iterative form becomes

$$\left[(1-M_\infty^2)\,\phi_{,x}^{n+1} - M_\infty^2\,\frac{(1+\gamma)}{2}\,\phi_{,x}^{n}\,\phi_{,x}^{n+1}\right]_{,x} + \phi_{,yy}^{n+1} = 0 \tag{10}$$

where n+1 denotes the variable ϕ to be solved for, and n denotes the variable ϕ calculated from the previous iteration.

The method of weighted residuals is a technique used to generate finite element equations when variational functions are not available. This method assumes an approximate solution of the form

$$\phi(X,Y) \simeq \hat{\phi} = \sum_{i=1}^{n} N_i(X,Y)\,\phi_i \tag{11}$$

where the N_i's are functions that satisfy boundary conditions and the ϕ_i's are the solutions at global node points i. Substituting this approximate solution into eq 10 results in the equation not being equal to zero, but now being equal to some error ε. As the error approaches zero, the approximate solution approaches the exact one. Therefore, the object is to get this error as small as possible. This is done in a weighted average sense by substituting ε into

$$\int_{\Omega} \varepsilon W_i \, d\Omega = 0 \tag{12}$$

where W_i is a weight or test function. Substituting for ϵ in eq 12 yields

$$\int_{\Omega} \left\{ \left[\left(1 - M_\infty^2 - M_\infty^2 \frac{1+\gamma}{2} \hat{\phi}_{,x}^{n} \right) \hat{\phi}_{,x}^{n+1} \right]_{,x} + \hat{\phi}_{,yy}^{n+1} \right\} W_i \, d\Omega = 0 \tag{13}$$

which is still second-order and requires N_i to be continuous through its first derivative (C^1). Integrating eq 13 by parts eliminates the C^1 continuity by shifting a derivative from $\hat{\phi}$ to W_i and thus requires $N_i(x,y)$ and $W_i(x,y)$ to only be continuous functions (C^0). The resulting equation after integration by parts is

$$\begin{aligned} &- \int_{\Omega} \left\{ \left[1 - M_\infty^2 - M_\infty^2 \frac{1+\gamma}{2} \hat{\phi}_{,x}^{n} \right] \hat{\phi}_{,x}^{n+1} W_{i,x} + \hat{\phi}_{,y}^{n+1} W_{i,y} \right\} d\Omega \\ &+ \int_{\partial\Omega} \left\{ \left[1 - M_\infty^2 - M_\infty^2 \frac{1+\gamma}{2} \hat{\phi}_{,x}^{n} \right] \hat{\phi}_{,x}^{n+1} n_x W_i + \hat{\phi}_{,y}^{n+1} n_y W_i \right\} dS = 0 \end{aligned} \tag{14}$$

where $\partial\Omega$ denotes the boundary and $\vec{n} = (n_x, n_y)$ is the unit normal vector to the boundary surface.

When evaluating the boundary term of eq 14, the integral must be broken down into a series of integrals over each of the six boundaries shown in Figure 6. Before evaluating these integrals, the boundary conditions, given by eq 3, for the governing differential equation must be put into a workable form. Recalling, the boundary conditions

$$\nabla\phi \longrightarrow 0 \quad \text{as} \quad r \longrightarrow \infty \tag{15}$$

and

$$\nabla\hat{\phi} \cdot \vec{n}_\alpha = 0 \qquad \text{along airfoil} \tag{16}$$

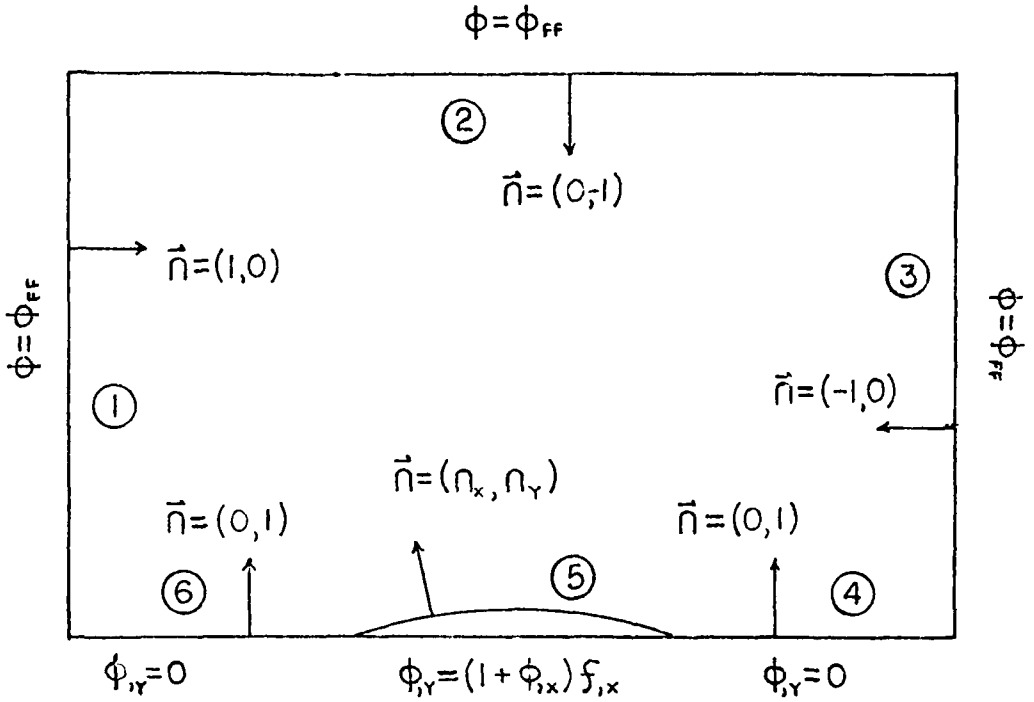

Figure 6. Flow Field Boundary Breakdown

where the full potential Φ is defined as

$$\Phi = U_\infty (X + \phi) \tag{17}$$

and $\vec{n}_\infty$ is the unit normal vector on the airfoil given by

$$\vec{n}_\infty = \frac{\nabla F}{\|\nabla F\|} = \frac{(f_{,x}, -1)}{\|\nabla F\|} \tag{18}$$

where

$$F = f(X) - Y = 0$$

is the equation of the airfoil given by eq 1. Substituting eqs 17 and 18 into eq 16 results in the boundary condition

$$\phi_{,y} = (1 + \phi_{,x}) f_{,x} \tag{19}$$

along the airfoil. From symmetry and steady flow in the x-direction another boundary condition

$$\phi_{,y} = 0 \tag{20}$$

exists for y=0 where $|x| \geq 1/2$.

In evaluating the boundary term of eq 14 for far field boundaries 1, 2, and 3, in Figure 6, the infinity boundary condition, given by eq 15, should be used. Since Klunker's boundary condition $\phi = \phi_{ff}$ given by eq 5 is used instead, then W_i will be taken to be zero there. The boundary terms due to segments 4 and 6, in Figure 6, are also zero when evaluated using $n_x = 0$ and eq 20. The only term that does not go to zero in the boundary term is for segment 5. Substituting eqs 18 and 19 into the boundary term of eq 14

results in

$$-\int_{\partial\Omega}\left\{\left[-M_\infty^2-M_\infty^2\frac{1+\gamma}{2}\hat{\phi}^n_{,x}\right]\hat{\phi}^n_{,x}W_i f_{,x}-W_i f_{,x}\right\}\Big|_{y=0} dX \tag{21}$$

Since ϕ and W_i will be continuous functions along inter-element boundaries, it is possible to integrate eq 14 piece-wise over the domain. Within each element, eq 11 for a four-noded rectangle, becomes

$$\hat{\phi}^{n+1}(X,Y)=\sum_{j=1}^{4}N_j(XY)\phi_j^{n+1}$$

or (22)

$$\hat{\phi}^{n}(X,Y)=\sum_{k=1}^{4}N_k(XY)\phi_k^{n}$$

where the N_j's and N_k's are now elemental shape functions. The shape function for a four-noded rectangular element is given in Appendix A. Substituting eqs 22 and 21 into eq 14, produce the finite element equations in elemental form. The equations, in the form described by eq 6, are

$$\left[(1-M_\infty^2)A_{ij}+B_{ij}-M_\infty^2\frac{1+\gamma}{2}C_{ij}(\phi^n)+M_\infty^2 D_{ij}\right.$$

$$\left.+M_\infty^2\frac{1+\gamma}{2}E_{ij}(\phi^n)\right]\phi_j^{n+1}=F_i \tag{23}$$

where

$$A_{ij}=\iint_\Omega W_{i,x}N_{j,x}\,dX\,dY$$

$$B_{ij}=\iint_\Omega W_{i,y}N_{j,y}\,dX\,dY$$

$$C_{ij}(\phi^n) = \phi_\kappa^n \iint_\Omega N_{\kappa,x} N_{j,x} W_{i,x}\, dX dY$$

$$D_{ij} = \int_{\partial\Omega_\alpha} N_{j,x}\, W_i\, f_{,x}\Big|_{y=0} dX \tag{24}$$

$$E_{ij}(\phi^n) = \phi_\kappa^n \int_{\partial\Omega_\alpha} N_{\kappa,x} N_{j,x}\, W_i\, f_{,x}\Big|_{y=0} dX$$

$$F_i = -\int_{\partial\Omega_\alpha} W_i\, f_{,x}\Big|_{y=0} dX$$

where $\partial\Omega_\alpha$ denotes that these terms apply only to elements on the boundary of the airfoil. These matrices are evaluated for the four-noded rectangular element in Appendices A, B, and C.

All of the parameters in eq 23 are specified except the weight function W_i. The reason for this, is that the weight function in this study, will change depending on the method used and whether an element is contained within the supersonic region. For all the upwind method elements in the subsonic region (elliptical), and for all the elements in the alternative integration method, Galerkin's method will be used. This means that for those cases, the weight function W_i will be the same as the shape function N_i. In the upwind method, the weight function for supersonic (hyperbolic) elements will be

$$W_i = N_i + \alpha U_i \qquad (25)$$

where U_i is an upwind function and α is a test coefficient. Both the upwind function method and the alternative integration method will be discussed in detail later in this section.

Transonic Problems

Chapter II explained what happens in the flow as transonic speeds are reached. This section explains how the phenomena will affect the finite element solutions.

Researchers studying the finite element (Refs 12, 13) and finite difference methods for transonic flow have reported convergence difficulties. Some believed the problem was in the small-disturbance potential equation (Ref 6), but Akay (Ref 12) reported convergence difficulties for the total potential equation. Others believed the problem was in the Galerkin formulation, because it does not account for the area of influence of supersonic nodes (Ref 5).

In the supersonic region, the governing equation is hyperbolic. From the aerodynamics of supersonic flow, a point in the flow cannot propagate waves forward; it can only be influenced by points that lie in a region inside the mach cone propagating forward, and can only influence points that are contained in the downstream cone. The mach cone is defined by the characteristic curves of the hyperbolic equation. It is believed that neglecting these phenomena leads to convergence difficulties using Galerkin's

method. For Galerkin's method, the nodes of an element are weighted the same when the upstream nodes should have more influence in supersonic elements.

In order to account for the hyperbolic behavior, researchers have tried various methods. In finite difference methods, special difference operators (backward differences) have been developed to insure convergence of the solution. In finite elements, there has not been a special formulation developed. Chan (Ref 13) changed the stiffness matrix for supersonic elements during the assembly process by zeroing out the rows in the stiffness matrix corresponding to nodes giving downwind influence. Chan's method gave converged results, but only for the least squares formulation. Marsh (Ref 5) modified the non-linear term $\phi_{,x}{}^{n}\phi_{,x}{}^{n+1}$ by putting in a relaxation term. His new term replaced $\phi_{,x}{}^{n}\phi_{,x}{}^{n+1}$ by $R\phi_{,x}{}^{n}\phi_{,x}{}^{n+1} + (1-R)\phi_{,x}{}^{n}\phi_{,x}{}^{n}U$, where R was the relaxation coefficient which ranged from 0 to 1, and U was an upwinding factor which also ranged from 0 to 1. The second term was then added to the forcing vector in the elemental equations. Marsh got converged solutions for mach numbers deep in the transonic range. His method worked quite well, the only difficulty encountered was selecting the values of R and U for any given freestream mach number. In this study, two new methods will be tried. One used by Christie (Ref 7), an upwind method, and the other suggested by Marsh, an alternative integration method.

Upwind Function Method

The purpose of the upwind function U_i is to weight the upstream nodes of supersonic elements more than the downstream nodes. The reason for this was explained previously in this section. The upwind function idea was taken from papers by Christie (Ref 7) and Heinrich (Ref 8). Christie applied upwind functions in second-order equations with significant first derivative terms, and Heinrich used it for the convective transport equation. Neither one of these parallels the transonic potential flow problem in this study, but the method seemed worthwhile to investigate.

Using Galerkin's method, the weight functions W_i are assumed to equal the shape functions N_i. Convergence problems arise when transonic flow is present, because the shape functions weight each node in an element the same. For elliptic elements (subsonic) Galerkin's methos ($W_i=N_i$) is used, but for hyperbolic and transition elements (supersonic) an upwind function is added to give

$$\begin{aligned} W_i &= N_i + \alpha U_i \qquad \text{(hyperbolic)} \\ W_i &= N_i + \beta U_i \qquad \text{(transition)} \end{aligned} \tag{25}$$

where U_i is the upwind function and α is a test coefficient. Transition elements are ones that contain both elliptic and hyperbolic nodes.

Shape Functions. Elemental shape functions N_i (Ref 1), must be equal to one at node i and zero at the other three

nodes. The shape functions for the bilinear rectangle used in this study are

$$N_i = \frac{1}{4}(1+\xi_i\xi)(1+\eta_i\eta) \tag{26}$$

where (ξ,η) are the variables in local coordinates, and (ξ_i,η_i) are the local coordinates of node i, i = 1,2,3,4. Figure 7 shows the relationship of shape functions within the element. By superposition, the nodal shape functions, eq 26, are added together to give the curve of the elemental shape function in Figure 8. Notice that the curve is constant over the element boundary. This shows that all the nodes are weighted the same.

Upwind Function. The purpose of the upwind function is to weight the upstream part of an element in the supersonic region more than the downstream part. This will be done by making U_i a piecewise parabolic function of the form (see Fig 9)

$$U_i = \begin{cases} \frac{\xi_i}{4P_1}\left[(\xi-H_1)^2 + K_1\right](1+\eta_i\eta) & -1<\xi<0 \\ \\ \frac{\xi_i}{4P_2}\left[(\xi-H_2)^2 + K_2\right](1+\eta_i\eta) & 0<\xi<1 \end{cases} \tag{27}$$

where (H,K) are the coordinates of the vertex of the parabola and P is half of the latus rectum (twice the distance from the vertex to the focus). Figure 10 shows a plot of $W_i = N_i + \alpha U_i$ (α=1) so the effect of the upwind function can be seen. Notice, now the upstream part of the element is

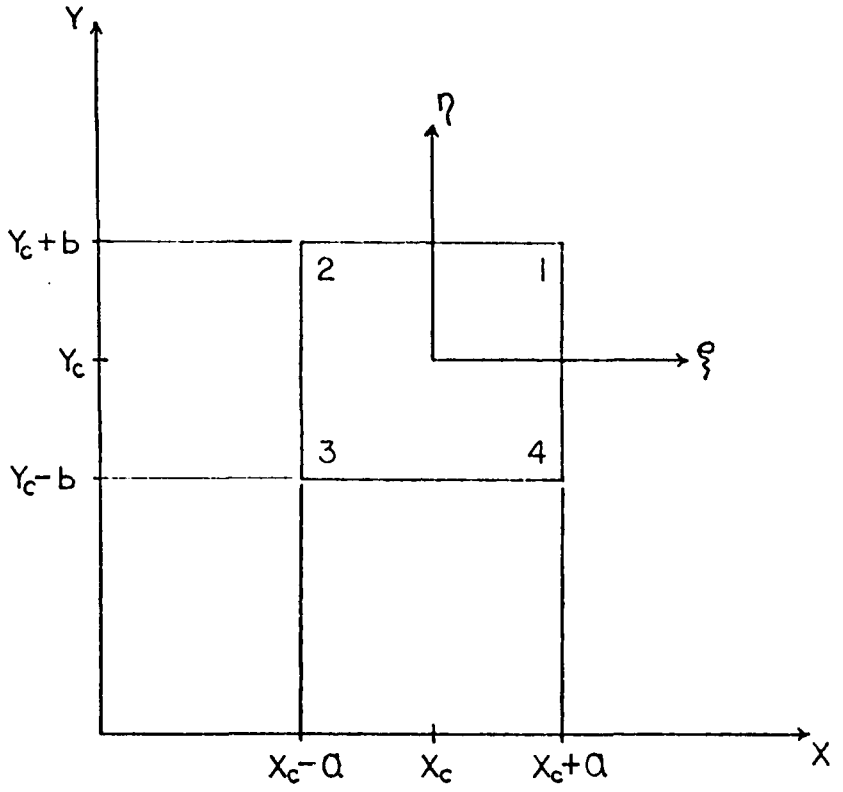

Figure 7. Local and Global Relationships for Bilinear Rectangular Element

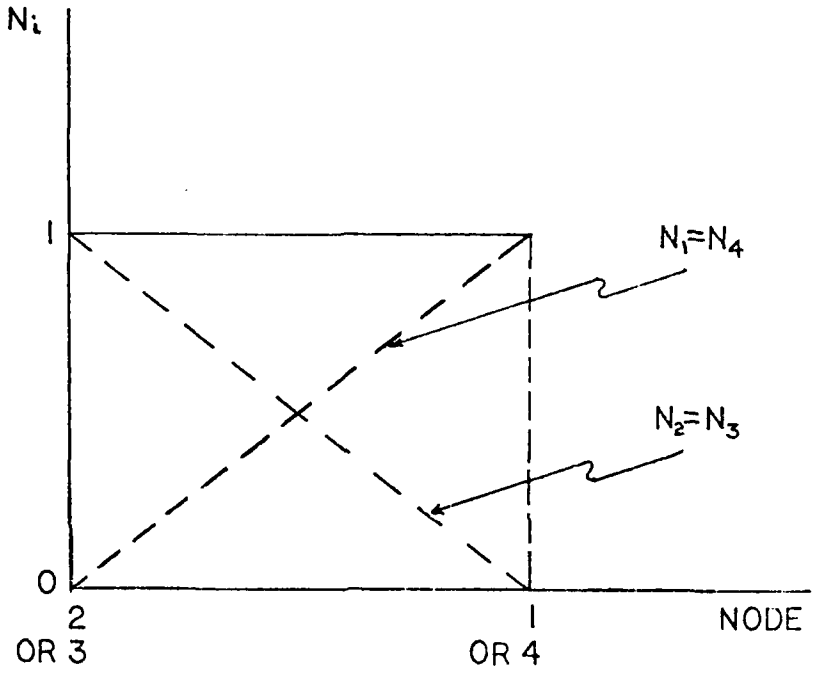

Figure 8. Relationship Between Nodal and Elemental Shape Functions

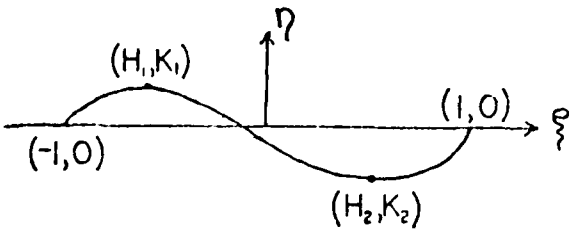

Figure 9. Piecewise Parabolic Upwind Function U_j

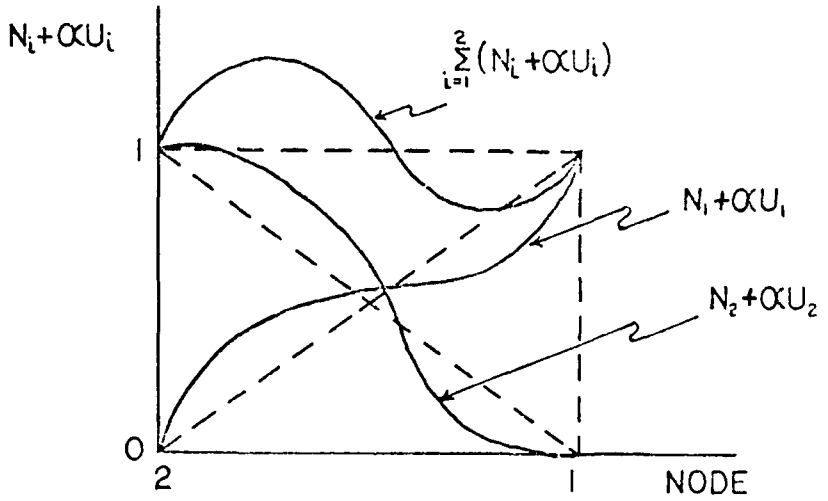

Figure 10. Effect of Upwind Function on Elemental Shape Function

weighted more than the downstream part.

Elemental Upwind Equations. Substituting $W_i = N_i + \alpha U_i$ into the elemental equation, given by eq 23, yields a new set of equations to be used for hyperbolic elements:

$$\left[(1-M_\infty^2)(A_{ij}+\alpha AU_{ij}) + B_{ij} + \alpha BU_{ij} - M_\infty^{2\frac{1+\gamma}{2}}(C_{ij}+\alpha CU_{ij})\right.$$

$$\left. + M_\infty^2(D_{ij}+\alpha DU_{ij}) + M_\infty^{2\frac{1+\gamma}{2}}(E_{ij}+\alpha EU_{ij})\right]\{\phi_j\} = -(F_i + \alpha FU_i) \tag{28}$$

where A_{ij}, B_{ij}, C_{ij}, D_{ij}, E_{ij}, and f_i were defined by eqs 24 and

$$AU_{ij} = \iint_\Omega N_{j,x} U_{i,x}\, dx\, dy$$

$$BU_{ij} = \iint_\Omega N_{j,y} U_{i,y}\, dx\, dy$$

$$CU_{ij}(\phi^n) = \phi_k^n \iint_\Omega N_{k,x} N_{j,x} U_{i,x}\, dx\, dy$$

$$DU_{ij} = \int_{\partial\Omega_\alpha} N_{j,x} U_i f_{,x}\Big|_{y=0} dx \tag{29}$$

$$EU_{ij}(\phi^n) = \phi_k^n \int_{\partial\Omega_\alpha} N_{k,x} N_{j,x} U_i f_{,x}\Big|_{y=0} dx$$

$$FU_i = \int_{\partial\Omega_\alpha} U_i f_{,x}\Big|_{y=0} dx$$

where $\partial\Omega_\alpha$ again means this integral is only applied for elements on the airfoil. Appendix B evaluates eqs 29 in matrix form for a bilinear rectangular element.

For the upwind method, α=0 will be used for elliptic elements, and α greater than zero for hyperbolic elements. The elements that have some nodes elliptic and some hyperbolic (transition elements) will use a value of β greater than or equal to zero. Note that $\alpha = \beta = 0$ reverts the elemental upwind equations (eq 28) to the elemental equations given by eq 23.

Alternative Integration Method

This method is based upon physical intuition and uses Galerkin's method for all elements. A modification is made for hyperbolic elements; the integrals (eq 24) are integrated only over the element area contained inside the forward mach cone (i.e. not over the entire element as done in Appendix A).

To find the form of the elemental stiffness matrix, the equations of the mach lines must be found. The mach lines are given by the characteristic lines of the governing differential equation given by eq 2 as

$$\phi_{,yy} + \frac{1}{c^2}\phi_{,xx} = 0 \qquad (30)$$

where $1/c^2 = 1 - M_\infty^2 - M_\infty^2(1 + \gamma)\phi_{,x}^{n}$. Since $u = \phi_{,x}$ can be calculated from the previous iteration and the element is small compared to the flow field, $1/c^2$ will be assumed constant. When the $\phi_{,xx}$ term is negative, eq 30 becomes

$$\phi_{,yy} - \frac{1}{C^2}\phi_{,xx} = 0 \qquad (31)$$

which is hyperbolic. With $1/c^2$ constant, the characteristic lines (Ref 10) are defined as

$$Y = CX + d \quad ; \quad Y = -CX + d \qquad (32)$$

which must now be transformed to local coordinates by the transformation equations

$$\xi = \frac{X - X_c}{a} \quad \text{and} \quad \eta = \frac{Y - Y_c}{b}$$

where x_c, y_c, a, and b are shown in Figure 7. The characteristic (mach) lines now take the form

$$\eta = M\xi + B \quad ; \quad \eta = -M\xi + B \qquad (33)$$

where

$$M = C\frac{a}{b}$$

$$B = C\frac{x_c}{b} + \frac{d}{b} - \frac{y_c}{b}$$

Now that the equations for the mach cone are known for any point in the supersonic region, the influence on the stiffness matrix [K] can be determined. K_{ij} is defined (Ref 1) as the force at node i due to the unit potential at node j. Therefore, only terms in which node i falls into the mach cone at point j have influence in the solution.

When an element aspect ratio b/a is greater than or equal to the slope c of the mach lines, the elements take the form shown in Figure 11a and its stiffness matrix takes the form

$$\begin{bmatrix} K_{11} & 0 & 0 & 0 \\ K_{21} & 0 & 0 & K_{24} \\ K_{31} & 0 & 0 & K_{34} \\ 0 & 0 & 0 & K_{44} \end{bmatrix}$$

Similarly, when b/a is less than c, see Figure 11b, the stiffness matrix is

$$\begin{bmatrix} K_{11} & 0 & 0 & 0 \\ K_{21} & 0 & 0 & 0 \\ 0 & 0 & 0 & K_{34} \\ 0 & 0 & 0 & K_{44} \end{bmatrix}$$

where K_{ij} in both cases is calculated for a bilinear rectangular element in Appendix C.

Transition elements pose more of a problem, because a linear interpolation scheme must be imposed to find the value of η^* where the element changes from hyperbolic to elliptic. If the slope of the characteristic curve passes through $\xi = -1$ below η^*, that intercept must be used as the limit of integration in the η-direction, otherwise, η^* will be used. In either case the element shown in Figure 11c has a stiffness matrix of the form

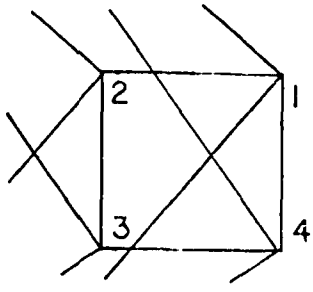

a) Supersonic Element c > a/b

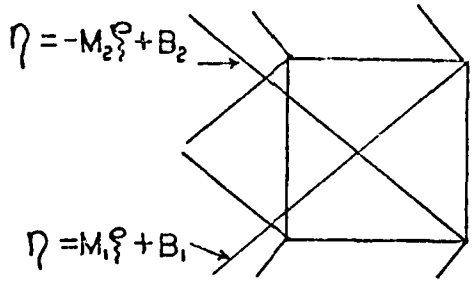

b) Supersonic Element c < a/b

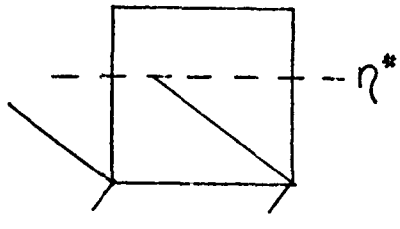

c) Transition Element

Figure 11. Mach Cones at Nodes of Supersonic and Transition Elements

$$\begin{bmatrix} K_{11} & K_{12} & 0 & 0 \\ K_{21} & K_{22} & 0 & 0 \\ 0 & 0 & 0 & K_{34} \\ 0 & 0 & 0 & K_{44} \end{bmatrix}$$

Again, Appendix C calculates the values for K_{ij}.

Summarizing the alternative integration method, the elliptic elements use Galerkin's method integrated over the entire element. The hyperbolic and transition elements are integrated over the area inside the forward mach cone. For example, for b/a<c, the limits of integration for K_{21}, for the area shown in Figure 12, are

$$\int_{-1}^{1} \int_{M_1\xi+B}^{1} F(\xi,\eta)\, d\eta\, d\xi$$

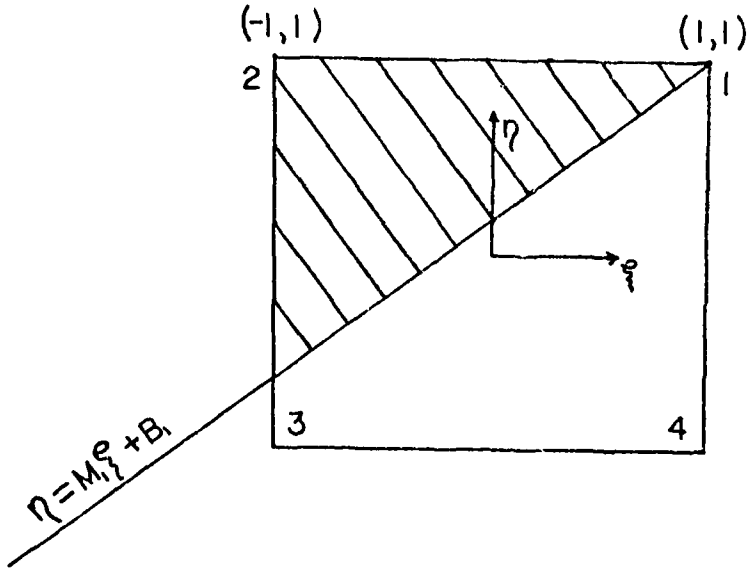

Figure 12. Area of Integration for K_{21} Term

IV Results

Transonic flow over a six percent thick airfoil was solved for using the two upwind techniques described in Chapter III. For each technique, different parameters were varied in order to study the convergence behavior of the solution. Before the transonic cases were tried, the incompressible (M_∞=0) case and subsonic cases were tried to see if the finite element equations defined in Appendix A accurately modeled the flow.

For incompressible flow, the solution shown in Figure 13 was found by directly solving the finite element equation. This solution is compared with the exact solution (Fig 13) for two discretizations. Grid A was the same as shown in Figure 5 and Grid B was similar, except it had ten divisions over the airfoil instead of eight. Taking the value of the coefficient of pressure in an element to be at the mid point between nodes, Figure 14 shows that the finite element solution closely approximates the exact solution.

Subsonic cases were tried for freestream mach numbers between 0.2 and 0.8. All these cases were below the critical mach number M_{cr}, and converged within four iterations. They also agree with linear theory until M_∞ got near 0.8, when the non-linear term started to show its effect. Figure 15 shows the pressure distribution for M_∞=0.2, 0.4, 0.6, 0.8, and Figure 16 shows the difference between the linear (Ref 6)

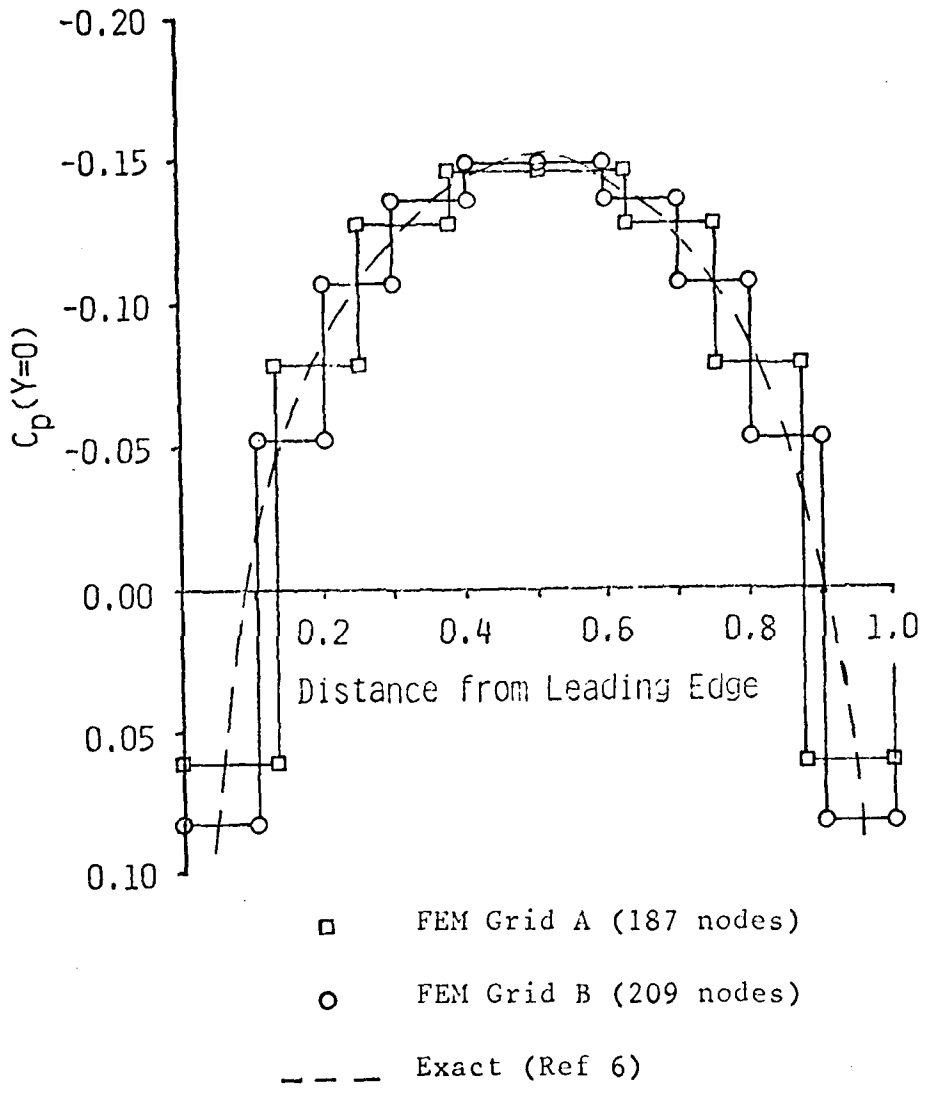

Figure 13. Finite Element Solution ($C_p(y=0)$) for Incompressible Flow Over a 6% Thick Airfoil

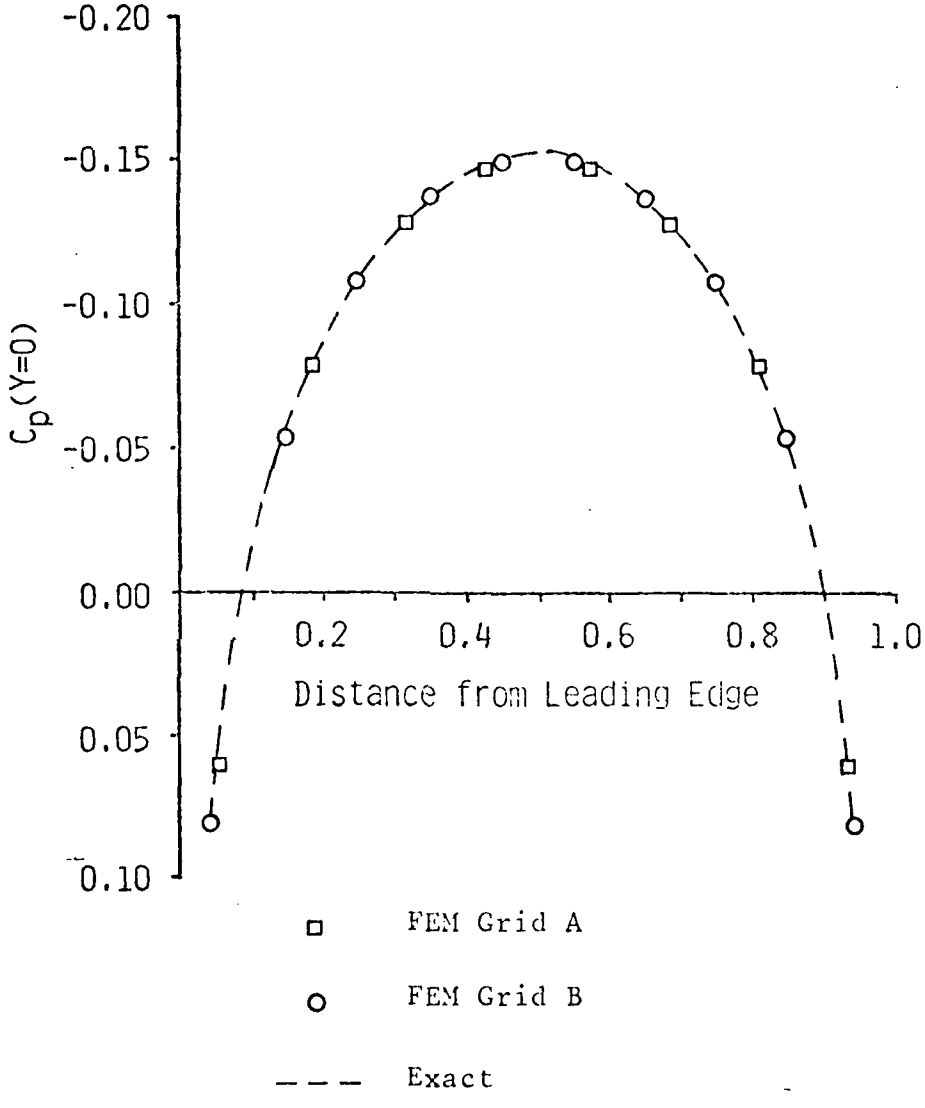

Figure 14. Finite Element Solution Compared to Exact for M_∞=0, 6% Thick Airfoil

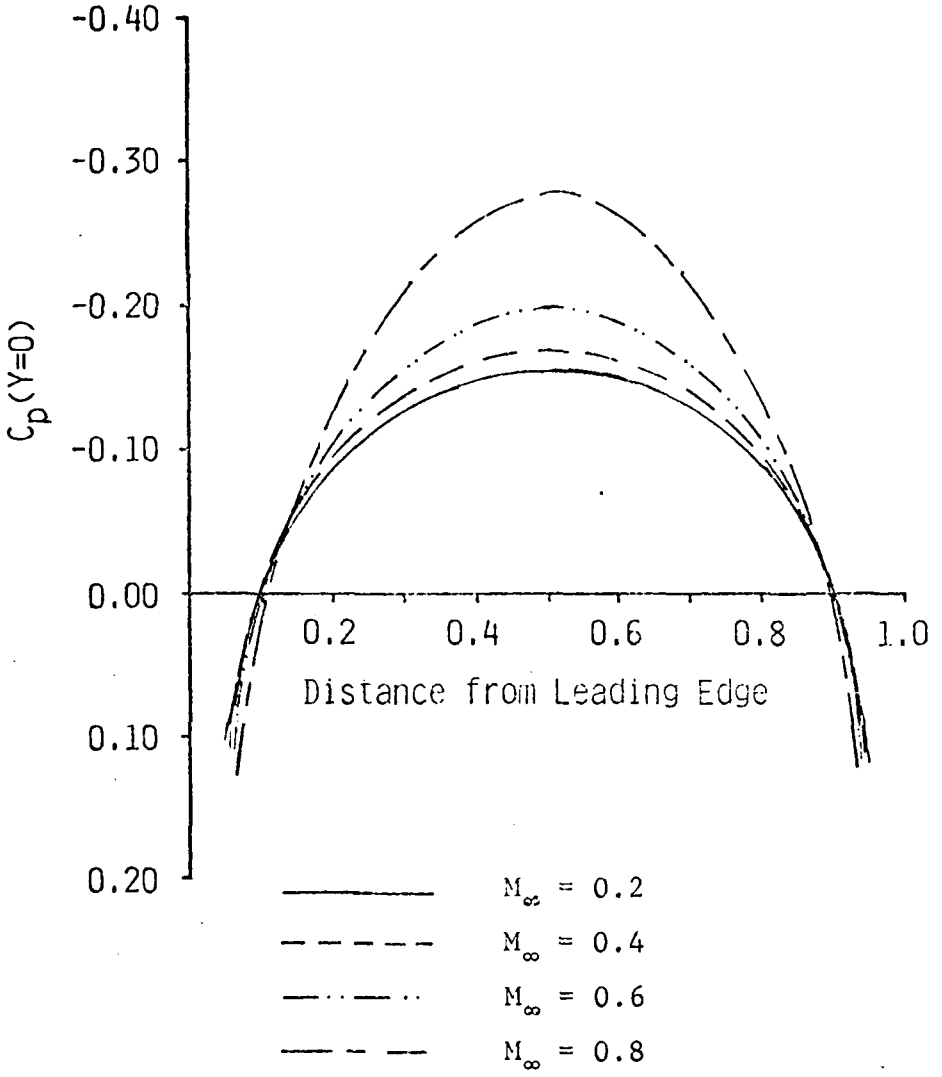

Figure 15. Mach Effects on (p(y=0)) for 6% Parabolic Airfoil

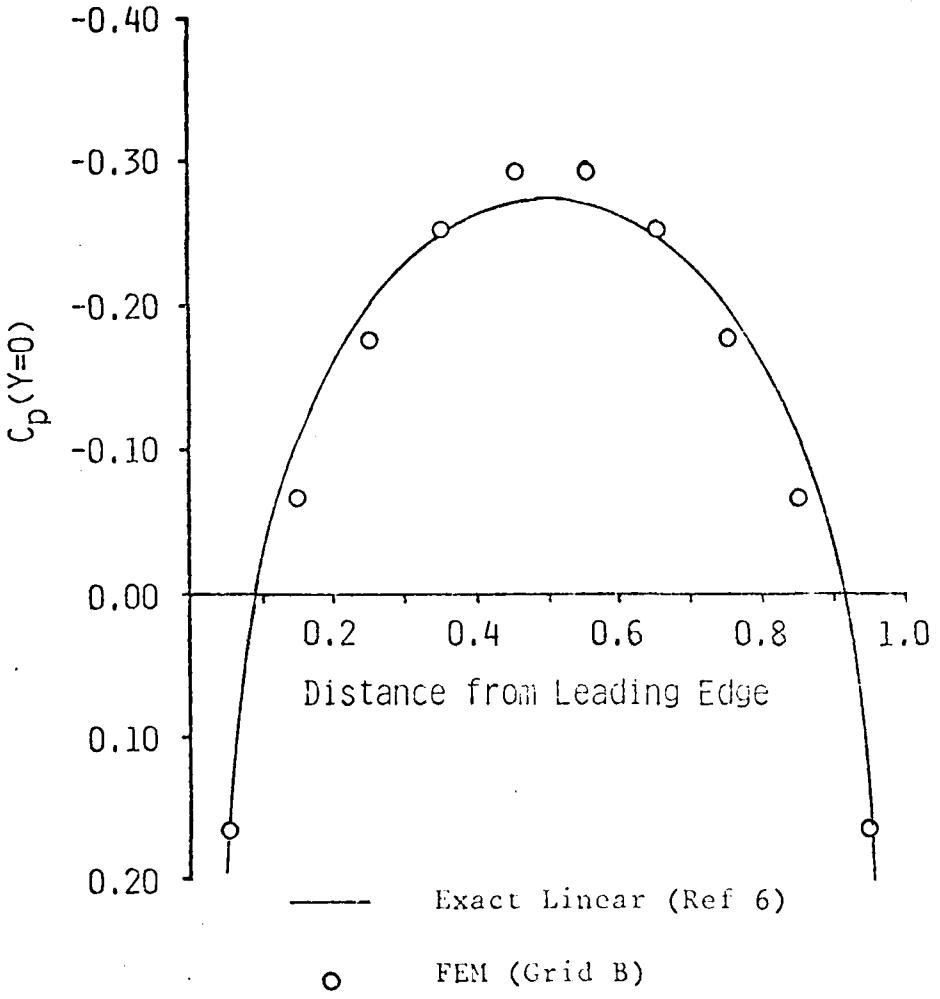

Figure 16. Comparison of Finite Element and Exact Linear Solutions for M_∞=0.8

and finite element solutions for M_∞=0.8. Notice that the difference between solutions is slight, even at M_∞=0.8.

Using Galerkin's method, without upwind techniques, mach numbers above 0.8 were run to find the critical value of M_∞. Figure 17 shows the pressure distributions found for the mach numbers that converged. The critical free-stream mach number was found to be between M_∞=0.83 and 0.84 for a six percent thick parabolic airfoil. Notice that the solution does converge for M_∞=0.84 and 0.85. This is because the supersonic region is small. Figure 18a,b shows the transition and hyperbolic element in the flow field for M_∞=0.84 and 0.85.

In Figures 19 and 20, convergence behavior is shown using Galerkin's method for M_∞=0.85 and M_∞=0.86. At M_∞=0.85 the solution converged after seven iterations, and at M_∞=0.86, the solution diverged because of the presence of two hyperbolic and four transition elements. As the free-stream mach number increased from zero to 0.85, the number of iterations required to get a converged solution increased, and above M_∞=0.85, the iterative scheme diverged. This behavior is graphed in Figure 21 for convergence criteria in the sense of eq 9.

These calculations proved that the finite element method as formulated worked until transonic flow developed. The techniques discussed in Chapter III were then tried to see if convergent solutions occur for $M_{cr} < M_\infty < 1.0$ which is in the transonic region. The rest of this section discusses the

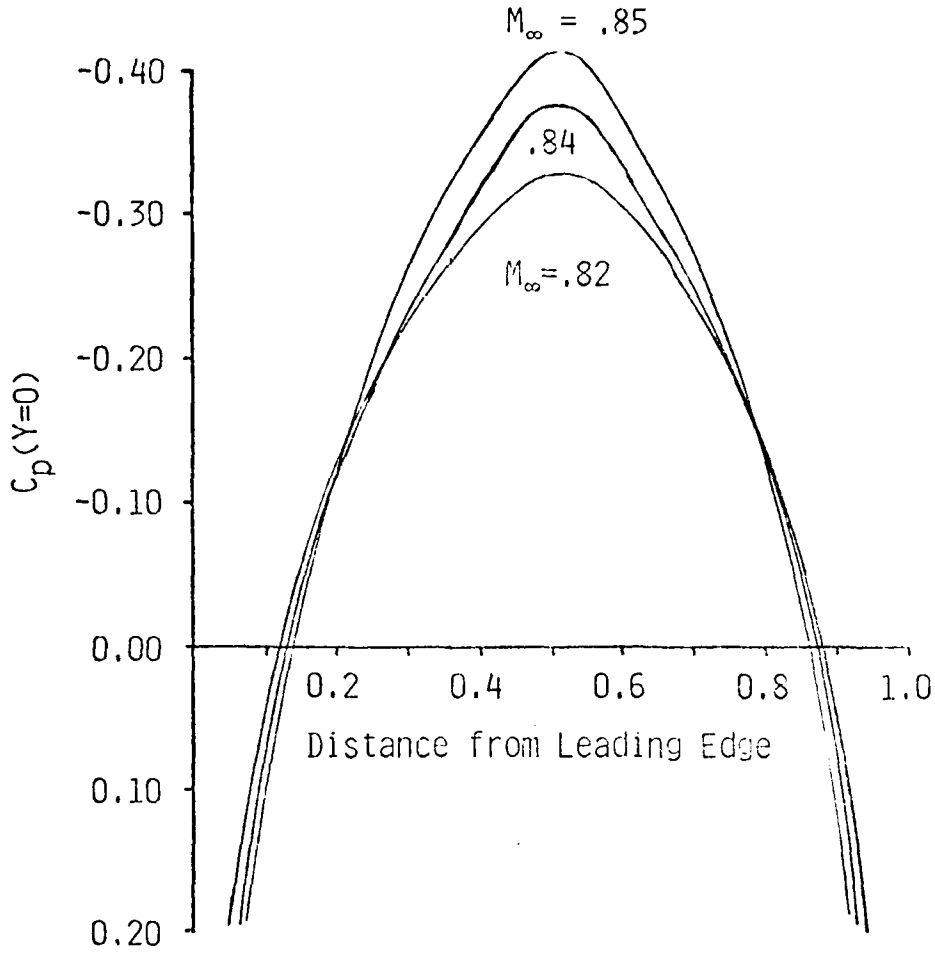

Figure 17. Convergent Results for M_∞=.82, .84, .85 with a 6% Thick Airfoil

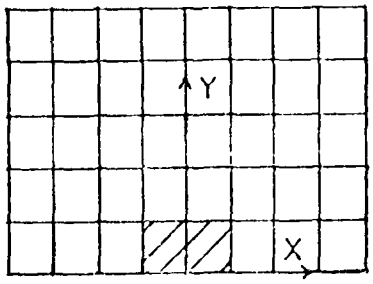

a) $M_\infty = 0.84$

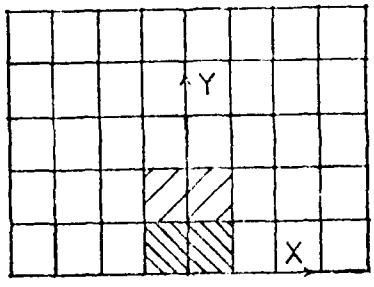

b) $M_\infty = 0.85$

Figure 18. Element Type and Location Over Thin Airfoil for $M_\infty = 0.84, 0.85$

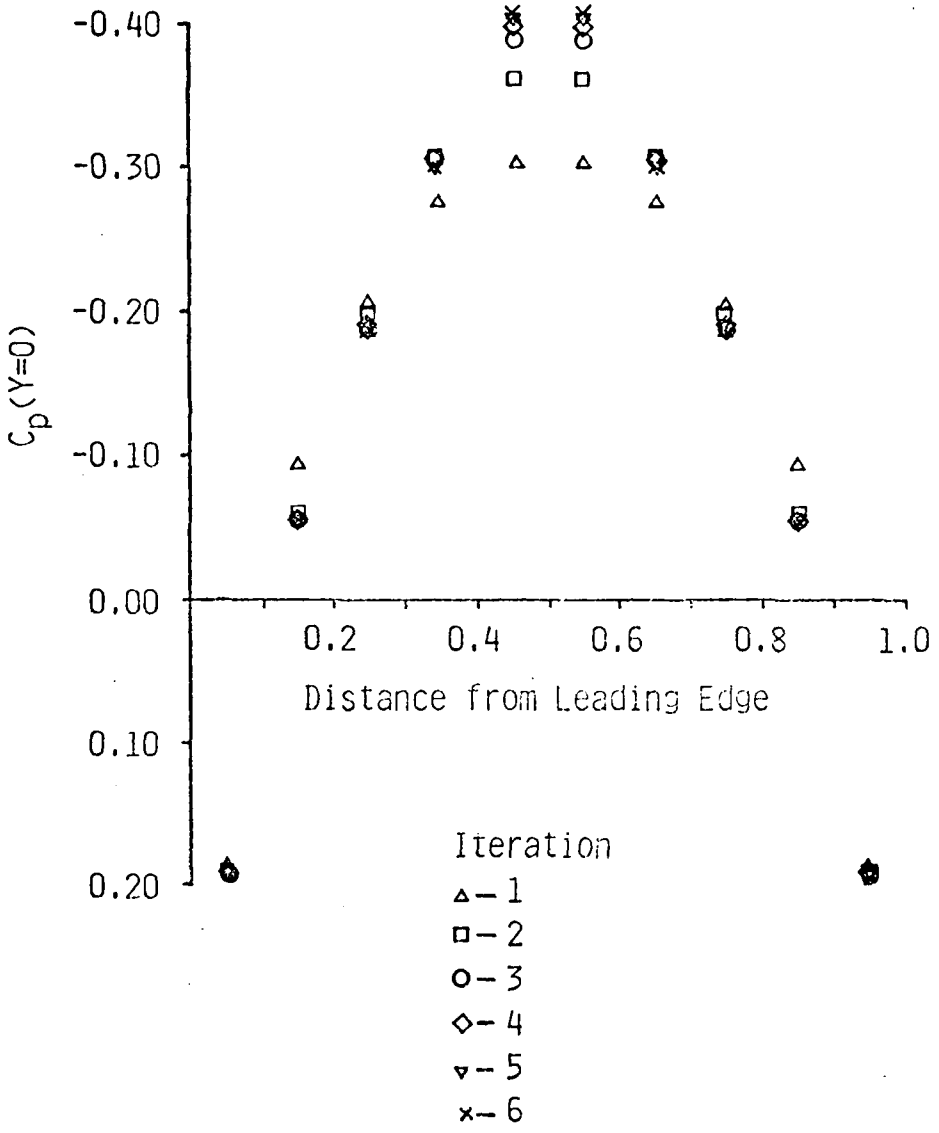

Figure 19. Iterative Convergence Behavior for $M_\infty = 0.85$

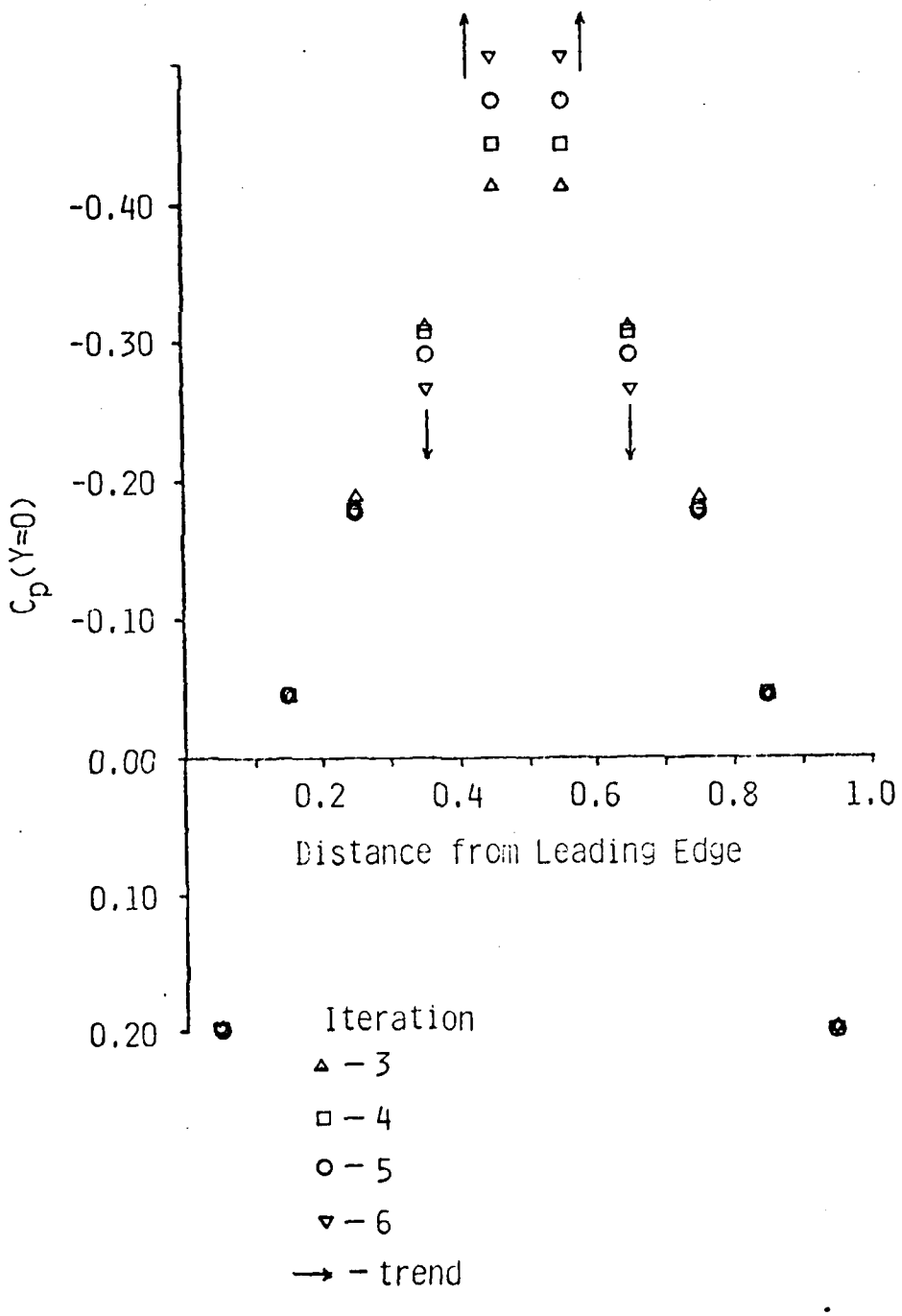

Figure 20. Iterative Divergence Behavior for $M_\infty = 0.86$

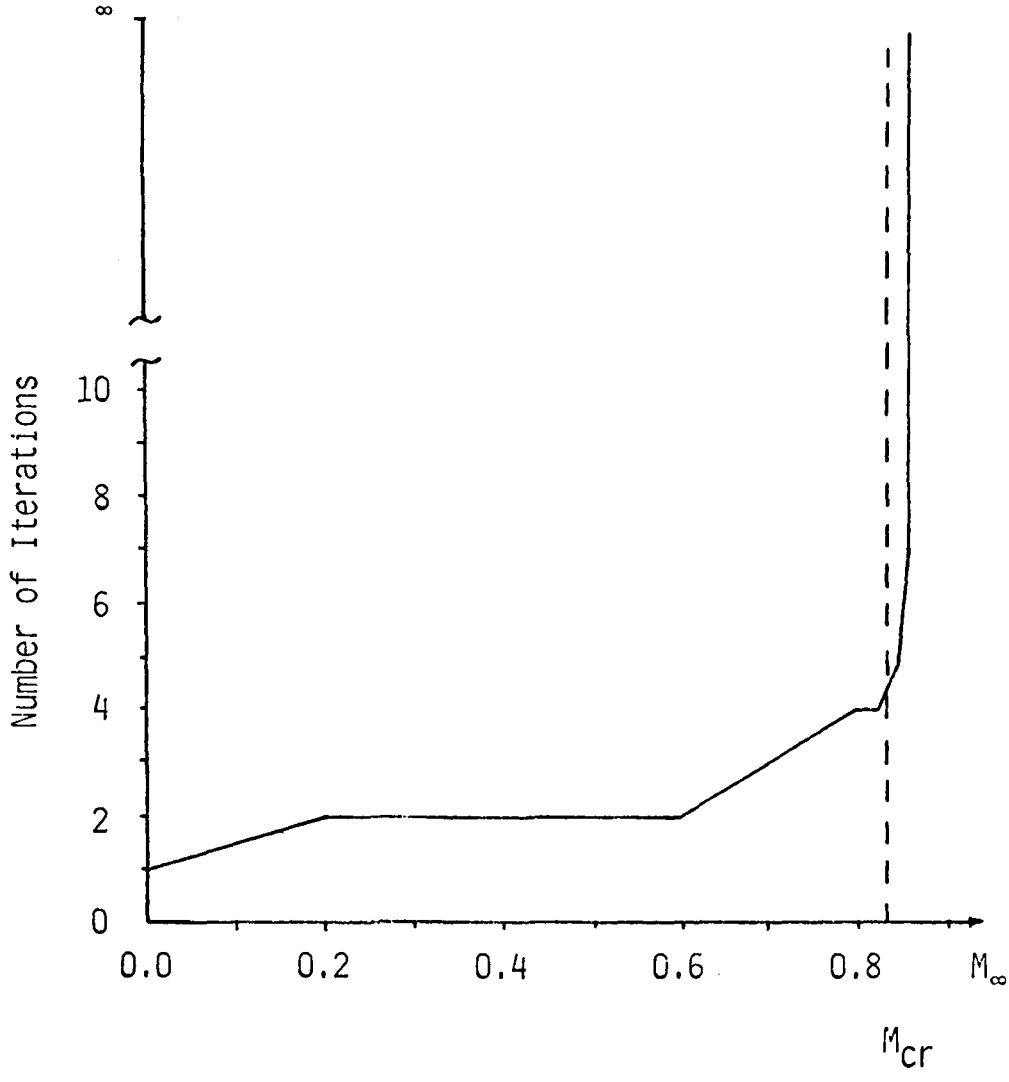

Figure 21. Convergence Behavior as a Function of M_∞ for a 6% Thick Parabolic Airfoil

results obtained for the upwind and alternative integration methods.

Upwind Method

The upwind function method discussed in Chapter III was tried for several variations of the test coefficients α and β, the area under the upwind function curve, the freestream mach number M_∞, and the y-direction upwind influence (BU_{ij}).

Y-Direction Influence. The upwind functions given by eq 27, are only functions of x, and do not affect the y-direction. The reason for this, is that the freestream flow is parallel to the x-axis. Because of this, the y-direction contribution to the elemental upwind equations can be neglected. The only term in the elemental upwind equations, given by eqs 28 and 29, that is related to the y-direction is the BU_{ij} term. Whenever this term was included in the elemental stiffness matrix, the solution diverged, or at best oscillated about some solution.

Test Coefficient Influence. The test coefficients α, β appear in eq 25 as

$$W_i = N_i + \alpha U_i \qquad \text{for hyperbolic elements}$$

and

$$W_i = N_i + \beta U_i \qquad \text{for transition elements}$$

Their purpose was to vary the strength of the upwind function in order to achieve convergence. The full influence of α

and β cannot be expressed without considering the upwind function itself, but some generalizations can be made. First, it was found that whenever either of these values was greater than one or less than zero, the solutions for any upwind function diverged rapidly. Also, whenever the value of β for transition elements was greater than α for hyperbolic elements, the solution again diverged rapidly. The solutions that used a value of β, one half the value of α seemed to have better solutions, but this depended on the mach number and the upwind function used. These effects will be incorporated in the subsection on different upwind functions.

Mach Number Effects. The value of the freestream mach number M_∞ had a large effect on the convergence of the solution. When $M_\infty > 0.87$, convergence never occurred for all upwind functions and test coefficients tried. For $M_\infty < 0.87$, convergent solutions were obtained, but depended on the upwind function parameters and test coefficients. The details are presented in the next subsection.

Upwind Function Influence. The equations for the upwind function, given by eq 27, are

$$\frac{f_i}{4P_1}(\xi - H_1)^2 + K_1 = 0 \qquad -1 < \xi < 0$$

$$\frac{f_i}{4P_2}(\xi - H_2)^2 + K_2 = 0 \qquad 0 < \xi < 1$$

The vertex of the piecewise parabolas (H,K) can vary.

Examples of different upwind function parameters are shown in Figure 22. For explanation purposes, the area above the ξ-axis will be called the positive area, and the area under the ξ-axis will be referred to as the negative area.

In all three cases of Figure 22, upwinding is present, whether it be more influence from the upstream part of an element, or less influence from the downstream part. It was found, that whenever the amount of positive area was greater than the amount of negative area, Figure 22a, a divergent solution occurred. This happened no matter what value of α and β were used. Pressure plots of divergent solutions are not very informative except to see where the divergence took place; so they will not be shown. In most cases, divergence occurred only where hyperbolic elements were present.

When the positive and negative areas were equal, Figure 22b, the solution was found to be oscillatory for certain values of α and β. For α less than one, all solutions diverged no matter what value of β was used. When α was equal to one, and $0.1 \leq \beta \leq 0.9$, oscillatory solutions for $0.25 \leq K_1 \leq 0.5$ and divergent solutions for other K_1 values where found. The oscillatory solution in Figure 23 is representative of what happened for equal area upwind functions with $\alpha=1$, $0.1 \leq \beta \leq 0.9$ and $0.25 \leq K_1 \leq 0.5$.

When the negative area was greater than the positive area, Figure 22c, convergent solutions occurred for certain values of $H_1, H_2, K_1, K_2, \alpha, \beta$ and M_∞. Varying H_1, H_2, K_1, K_2 resulted in

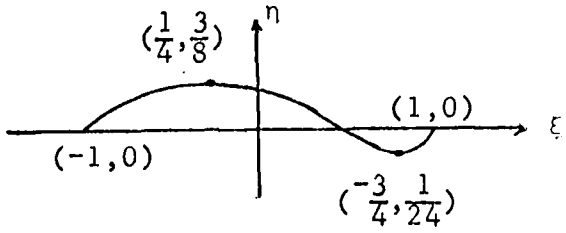

a) More Positive Influence on Upstream Nodes

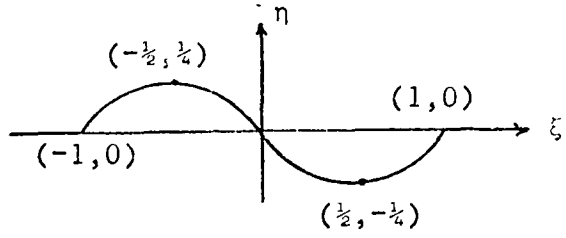

b) Positive Influence on Upstream Nodes with Equal Negative Influence on Downstream Nodes

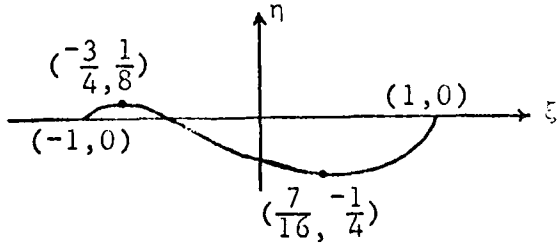

c) More Negative Influence on Downwind Nodes

Figure 22. Upwind Functions for Three Different Parameters of (H,K)

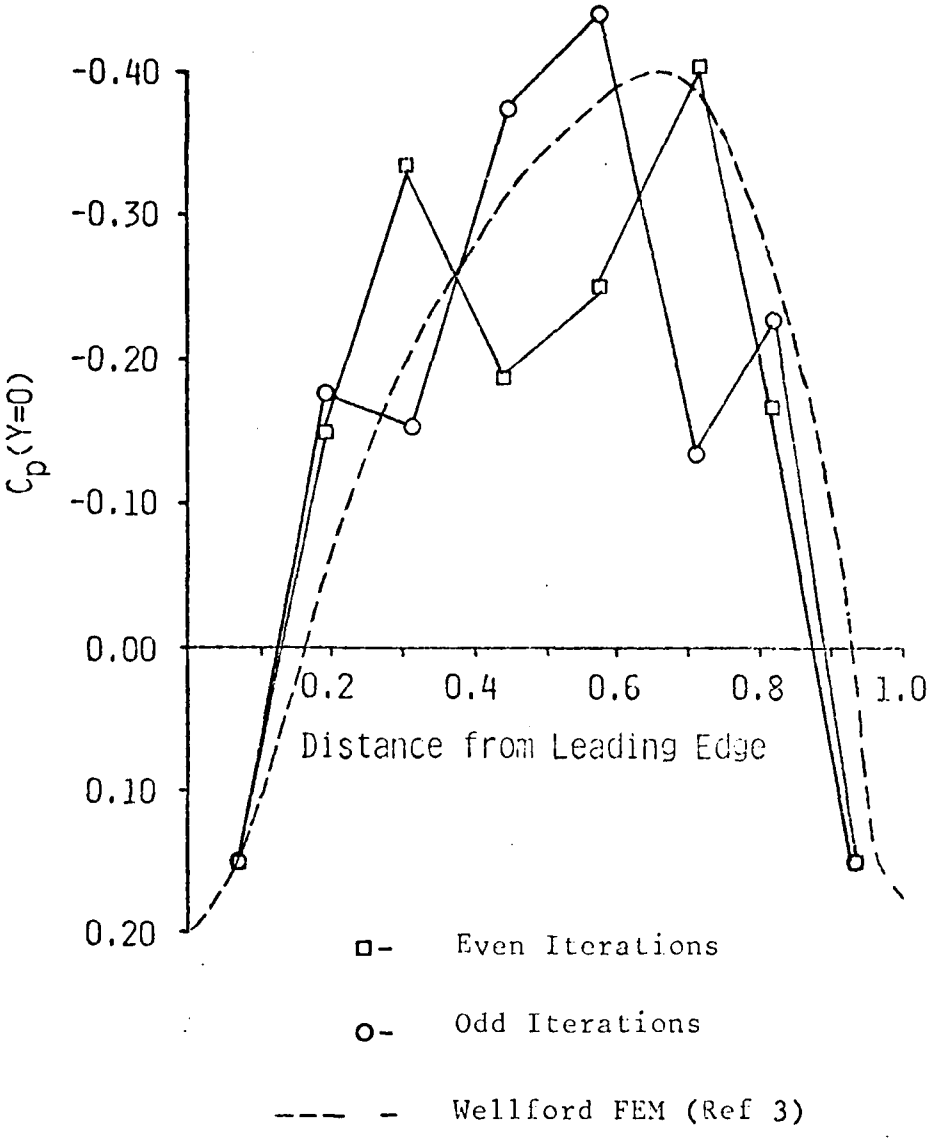

Figure 23. Oscillatory Solution for Equal Area Upwind Function (Grid A): M_{∞}=0.86

one combination that converged, and is shown in Figure 22c. Using this combination converged solutions occurred at M_∞= 0.86, α=1.0, β=0.5 and M_∞=0.86, α=0.5, β=0.5. All other combinations diverged or oscillated. These two converged solutions are shown in Figures 24 and 25.

Alternative Integration Method

The alternative integration method discussed in Chapter III was tried for a couple of cases. These included varying the mach number and the y-direction influence. The y-direction influence was varied by multiplying the BU_{ij} term of eq 29 by a coefficient ranging from zero to one. The mach number was ranged from 0.84 to 0.95.

In all cases, extremely divergent solutions resulted. The supersonic region expanded to the far field or physically unrealistic flow developed (i.e. supersonic flow developed upstream of the airfoil). Even when more elements were added to the grid over the airfoil, divergent solutions resulted. Figures 26 and 27 are representative of the effects of the grid size on the solution. Similar solutions resulted when the mach number and y-influence were varied.

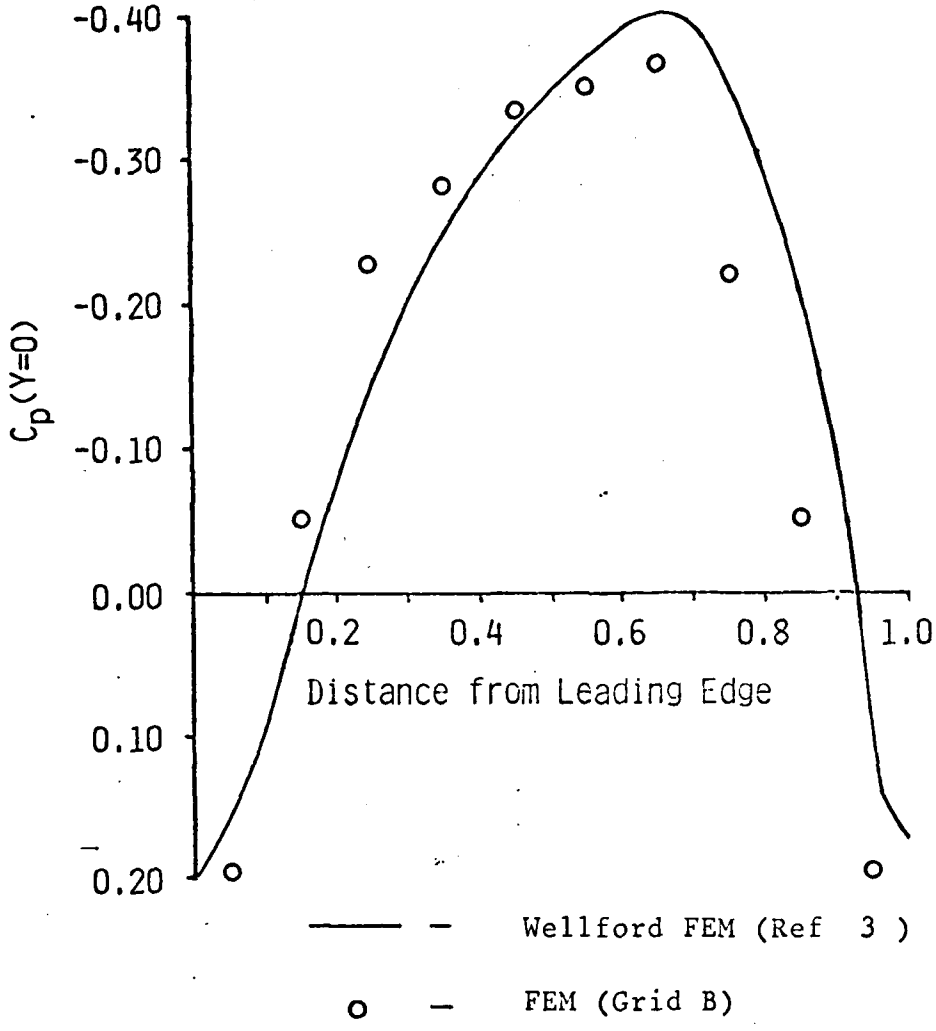

Figure 24. Converged Solution for M_∞=0.86, α=1.0, β=0.5

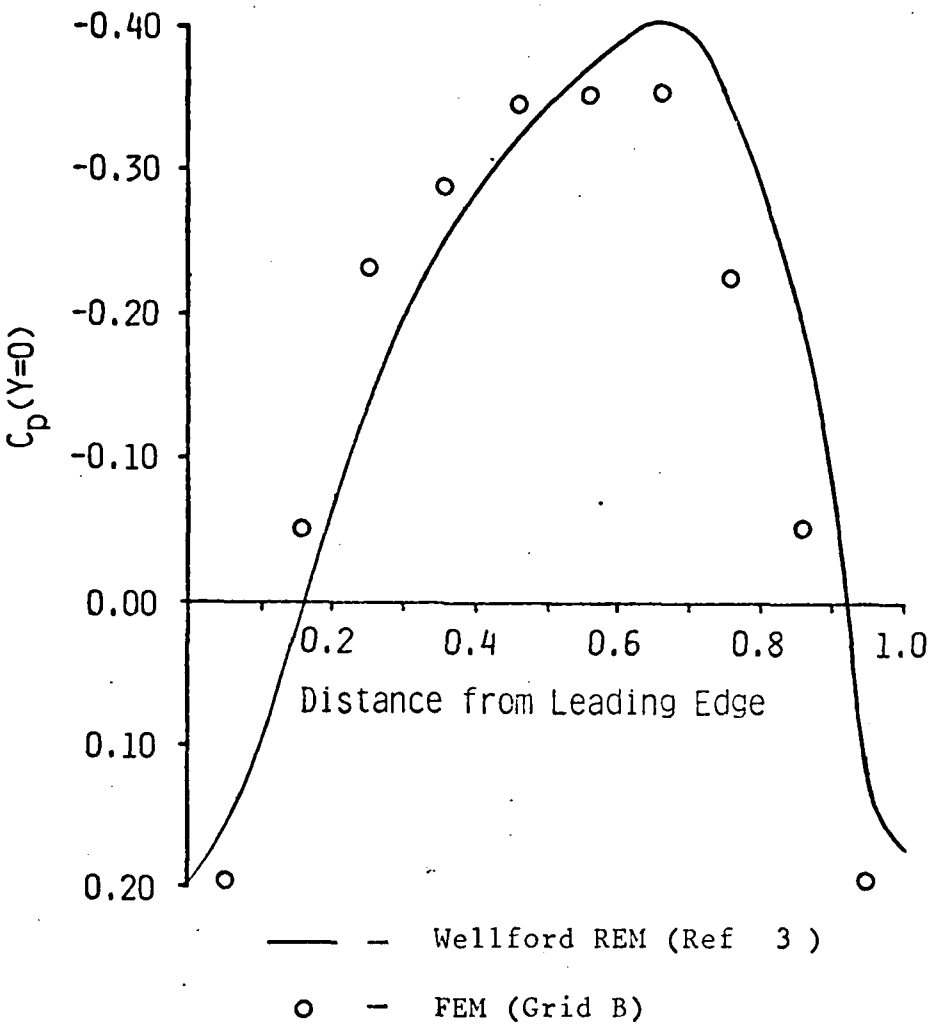

Figure 25. Converged Solution for M_∞=0.86, α=0.5, β=0.5

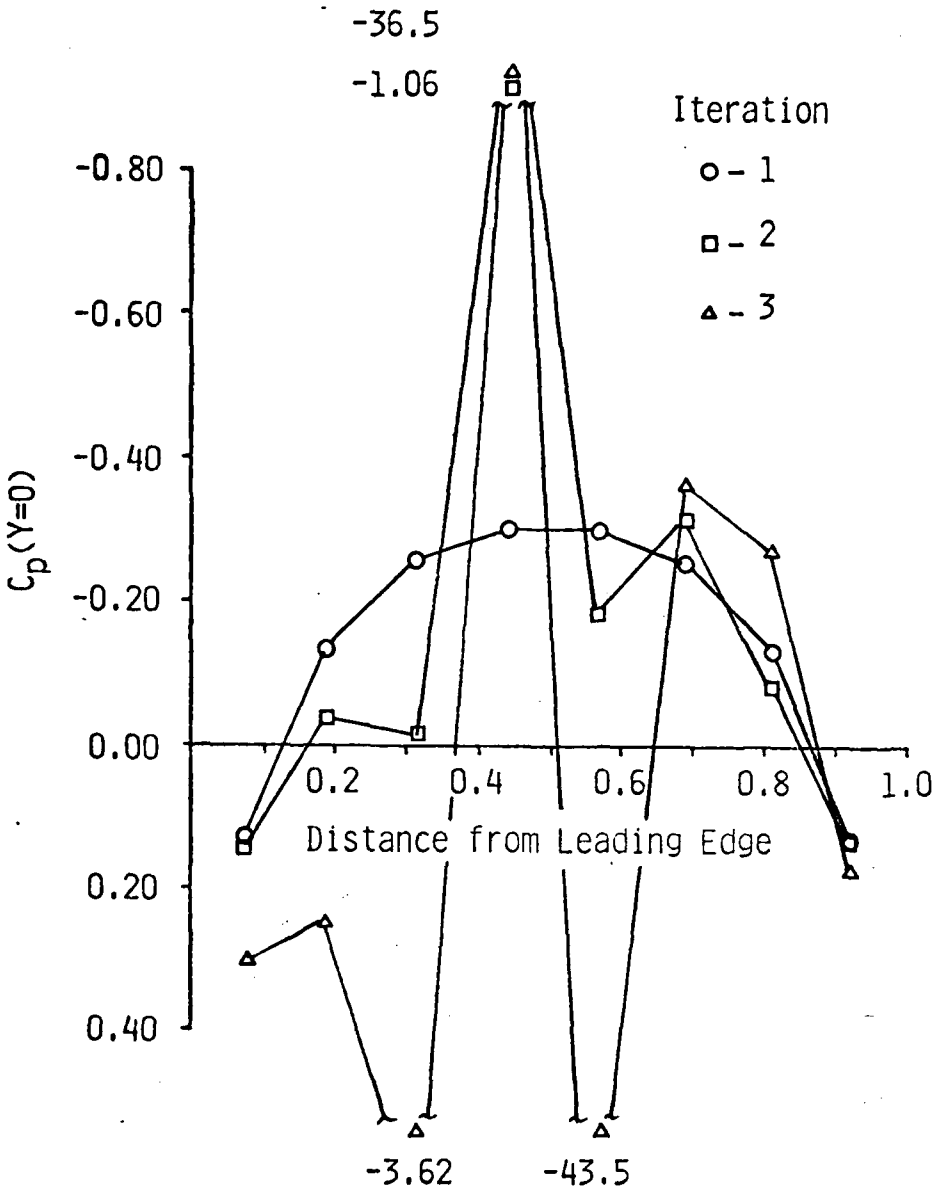

Figure 26. Divergent Solution Using Alternative Integration Method for Grid A

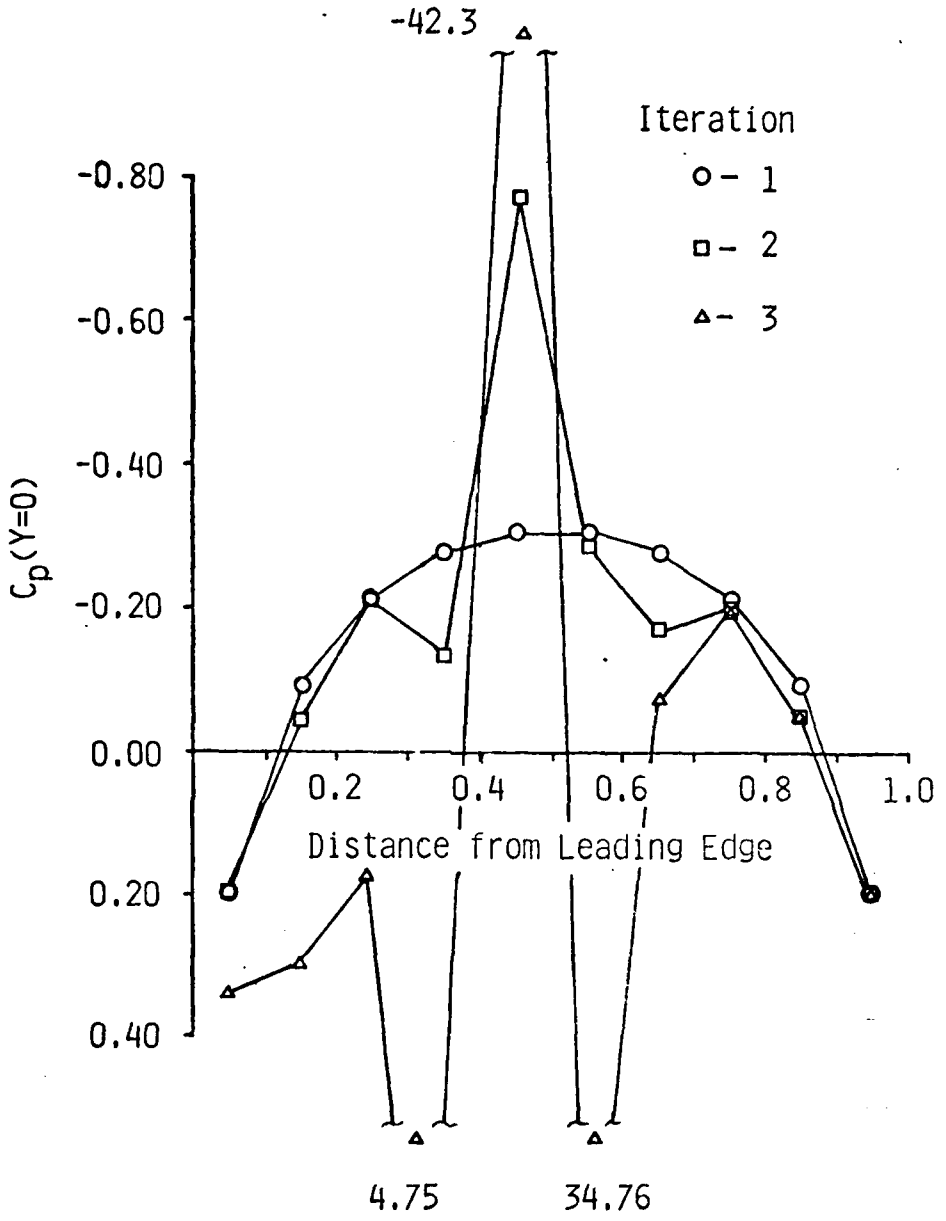

Figure 27. Divergent Solution Using Alternative Integration Method for Grid B

V. Conclusions and Recommendations

The upwind and alternative integration methods used in this study did not produce acceptable solutions to the small-disturbance potential equation for transonic flow. When the supersonic region covered more than two elements, the solution diverged, except for the cases of upwind parameters (H,K) shown in Figures 24 and 25.

Upwind Function

The upwind method, described in Chapter III, is not recommended for future use, because there are too many variables that must be optimized to get converged solutions. The solution depends on the freestream mach number M_∞, the upwind parameters (H_1,K_1), (H_2,K_2), and the test coefficients α and β. All of these must be incorporated in the finite element assembly process. It might be possible to use different upwind functions, such as piecewise linear or trigonometric functions instead of piecewise parabolic, and further study is warranted in this area.

Alternative Integration Method

This method gave divergent results for all cases, and as it stands, is not recommended for further study. Other approaches might be taken, for example, assembling the global stiffness matrix an equation at a time instead of an element at a time, the effect of nodes that have no influence on the solution could be zeroed out. Another

approach, could be to assume that the border between the super and subsonic regions be considered a boundary. Then solve the elliptical part, and using the solution on the border, apply it as a boundary condition when solving the hyperbolic part. This process would have to be done iteratively until the solution agreed on the boundary between the regions.

Bibliography

1. Zienkiewicz, O.C. The Finite Element Method. London: McGraw-Hill, 1977.

2. Shen, S.F. and Habashi, W.G. "Local Linearization of the Finite Element Method and its Application to Compressible Flows," International Journal for Numerical Methods in Engineering, 10: 565-577 (1975).

3. Wellford, L.C. and Hafez, M.M. "Implicit Velocity Formulation for the Calculation of Transonic Flow by the Finite Element Method," Proceedings of the Symposium on Applications of Computer Methods in Engineering. August 1977.

4. Hafez, M.M. et al. Finite Elements and Finite Differences for Transonic Flow Calculations. Kent, WA: Flow Research Co. May 1977.

5. Chan, S.K. and Brashears, M.R. Finite Element Analysis of Transonic Flow. AFFDL-TR-74-11. Wright-Patterson Air Force Base, OH: March 1974.

6. Marsh, J.E. Prediction of Aerodynamic Forces on a Circular Cylinder and a Thin Airfoil in a Transonic Airstream by the Finite Element Method. Wright-Patterson Air Force Base, OH: Air Force Institute of Technology, 1979.

7. Christie, I. "Finite Element Methods for Second Order Differential Equations with Significant First Derivatives," International Journal for Numerical Methods in Engineering, 10: 1389-1396, 1976.

8. Heinrich, J.C. et al. "An Upwind Finite Element Scheme for Two-Dimensional Convective Transport Equation," International Journal for Numerical Methods in Engineering, 11: 131-143, 1977.

9. Landahl, M.T. Unsteady Transonic Flow. Long Island City, NY: Pergamon Press, 1961.

10. Zachmanoglou, E.C. Introduction to Partial Differential Equations with Applications. Baltimore, MD: Williams and Wilkins, 1976.

11. Klunker, E.B. Contributions to Methods for Calculating the Flow About Thin Lifting Wings at Transonic Speeds --Analytical Expressions for the Farfield. NASA TD-D-6530: November 1971.

12. Akay, H.U. et al. "Finite Element Analysis of Compressible Flow," Proceedings of the Symposium on Applications of Computer Methods in Engineering. August 1977.

13. Chan, S.K. et al. Finite Element Analysis of Transonic Flows Over Thin Airfoils - Volume I, Final Report. AFFDL-TR-76-49. Wright-Patterson Air Force Base, OH: May 1976.

Appendix A

Finite Element Equations for a Bilinear Rectangular Element

Elemental Equations

The finite element equation for the governing differential equation in elemental form as derived in Chapter III is

$$\left[(1-M_\infty^2)A_{ij} + B_{ij} - M_\infty^2 \frac{1+\gamma}{2} C_{ij}(\phi^n) + M_\infty^2 D_{ij} + M_\infty^2 \frac{1+\gamma}{2} E_{ij}(\phi^n)\right] \phi_j^{n+1} = F_i \qquad \text{(A-1)}$$

where A_{ij}, B_{ij}, C_{ij}, D_{ij}, E_{ij} and F_i are defined by eqs 24.

Shape Functions

The shape functions (Ref 1) for the bilinear rectangular element shown in Figure 7 are given by

$$N_i = \frac{1}{4}(1+\xi_i\xi)(1+\eta_i\eta) \qquad i = 1,2,3,4 \qquad \text{(A-2)}$$

where (ξ_i, η_i) are the coordinates of the corner nodes in a local coordinate system (ξ, η). Since the elemental equations are expressed in global coordinates, they must be transformed to local coordinates by the transformation equations

$$\xi = \frac{X-X_c}{a} \quad \text{and} \quad \eta = \frac{Y-Y_c}{b} \qquad \text{(A-3)}$$

Substituting eqs A-3 into the elemental equations given by eq2 24 result in

$$A_{ij} = \frac{b}{a}\int_{-1}^{1}\int_{-1}^{1} N_{i,\xi}\, N_{j,\xi}\, d\xi\, d\eta$$

$$B_{ij} = \frac{a}{b}\int_{-1}^{1}\int_{-1}^{1} N_{i,\eta}\, N_{j,\eta}\, d\xi\, d\eta$$

$$C_{ij}(\phi^n) = \frac{b}{a^2}\phi_k^n \int_{-1}^{1}\int_{-1}^{1} N_{i,\xi}\, N_{j,\xi}\, N_{k,\xi}\, d\xi\, d\eta \qquad \text{(A-4)}$$

$$D_{ij} = \int_{-1}^{1} N_{j,\xi} N_i\, f_{i,x}(\xi)\Big|_{\eta=-1} d\xi$$

$$E_{ij}(\phi^n) = \frac{1}{a}\phi_k^n \int_{-1}^{1} N_{k,\xi} N_{j,\xi}\, N_i\, f_{i,x}(\xi)\Big|_{\eta=-1} d\xi$$

$$F_i = a\int_{-1}^{1} N_i\, f_{i,x}(\xi)\Big|_{\eta=-1} d\xi$$

where D_{ij}, E_{ij}, and f_i apply only to elements on the airfoil.

In eqs A-4, the A_{ij}, B_{ij} and C_{ij} terms depend only on the shape of the elements and not on their position. They can be integrated and evaluated for i = 1,2,3,4 and j = 1,2 3,4 to produce the following symmetric matrices:

$$A_{ij} = \frac{b}{3a}\begin{bmatrix} 1 & -1 & -\frac{1}{2} & \frac{1}{2} \\ & 1 & \frac{1}{2} & -\frac{1}{2} \\ & & 1 & -1 \\ & & & 1 \end{bmatrix}$$

$$B_{ij} = \frac{a}{3b}\begin{bmatrix} 1 & \frac{1}{2} & -\frac{1}{2} & -1 \\ & 1 & -1 & -\frac{1}{2} \\ & & 1 & \frac{1}{2} \\ & & & 1 \end{bmatrix}$$

$$C_{ij}(\phi^n) = \begin{bmatrix} C_{11} & -C_{11} & -C_{14} & C_{14} \\ & C_{11} & C_{14} & -C_{14} \\ & & C_{33} & -C_{33} \\ & & & C_{33} \end{bmatrix}$$

where

$$C_{11} = \frac{b}{8a^2}\left[\phi_1^n - \phi_2^n + \frac{1}{3}(\phi_4^n - \phi_3^n)\right]$$

$$C_{14} = \frac{b}{24a^2}\left[\phi_1^n - \phi_2^n + \phi_4^n - \phi_3^n\right]$$

$$C_{33} = \frac{b}{8a^2}\left[\frac{1}{3}(\phi_1^n - \phi_2^n) + \phi_4^n - \phi_3^n\right]$$

where the ϕ_i^n's are the solutions at node i from the previous iteration.

The remaining equations in A-4 are dependent on the position of the element. The quantities D_{ij}, E_{ij} and f_i exist only for elements that border the airfoil. These quantities are evaluated at $\eta = -1$, because a thin airfoil is being used. The equation of the airfoil is

$$Y = f(x) = \tau(1 - 4x^2) \qquad ; \ |x| \leq \frac{1}{2}$$

where τ is half thickness ratio. For this airfoil, E_{ij}, D_{ij} and f_i are evaluated to be

$$D_{ij} = 8\tau \begin{bmatrix} 0 & 0 & 0 & 0 \\ 0 & 0 & 0 & 0 \\ 0 & 0 & D_{33} & -D_{33} \\ 0 & 0 & -D_{44} & D_{44} \end{bmatrix}$$

$$E_{ij} = 8\tau \begin{bmatrix} 0 & 0 & 0 & 0 \\ 0 & 0 & 0 & 0 \\ 0 & 0 & E_{33} & -E_{33} \\ 0 & 0 & -E_{44} & E_{44} \end{bmatrix}$$

$$F_i = 8\tau a \begin{Bmatrix} 0 \\ 0 \\ 2D_{33} \\ -2E_{44} \end{Bmatrix}$$

where—

$$D_{33} = \frac{a}{2}\left[\frac{x_c}{a} - \frac{1}{3}\right]$$

$$D_{44} = -\frac{a}{2}\left[\frac{x_c}{a} + \frac{1}{3}\right]$$

$$E_{33} = \frac{1}{4}\left[(\phi_4^n - \phi_3^n)\left(\frac{x_c}{a} + \frac{1}{3}\right)\right]$$

$$E_{44} = \frac{1}{4}\left[(\phi_3^n - \phi_4^n)\left(\frac{x_c}{a} + \frac{1}{3}\right)\right]$$

Appendix B

Upwind Functions and Elemental Equations

In the upwind function method described in the text, the weight function is replaced by

$$N_i = N_i + \alpha U_i \tag{B-1}$$

in elemental equation 23, forming eq 28. The terms in the elemental upwind stiffness matrix and force vector (eq 29) with the limits of integration are

$$AU_{ij} = \int_{-1}^{1}\int_{-1}^{1} N_{j,x} U_{i,x}\, dx\, dy$$

$$BU_{ij} = \int_{-1}^{1}\int_{-1}^{1} N_{j,y} U_{i,y}\, dx\, dy$$

$$CU_{ij}(\phi^n) = \int_{-1}^{1}\int_{-1}^{1} \phi_k^n\, N_{k,x} N_{j,x} U_{i,x}\, dx\, dy$$

$$DU_{ij} = \int_{-1}^{1} N_{j,x}\, U_i\, f_{,x}\Big|_{y=0}\, dx \tag{B-2}$$

$$EU_{ij}(\phi^n) = \int_{-1}^{1} \phi_k^n\, N_{k,x} N_{j,x}\, U_i\, f_{,x}\Big|_{y=0}\, dx$$

$$FU_i = \int_{-1}^{1} U_i\, f_{,x}\Big|_{y=0}\, dx$$

Transforming eqs B-2 to local coordinates and substituting

$$U_i = \begin{cases} \frac{f_i}{4P_1}\left[(\xi - H_1) + K_1\right](1+\eta_i\eta) & -1<\xi<0 \\ \frac{f_i}{4P_2}\left[(\xi - H_2) + K_2\right](1+\eta_i\eta) & 0<\xi<1 \end{cases}$$

and

$$N_i = \frac{1}{4}(1+\xi_i\xi)(1+\eta_i\eta)$$

results in

$$AU_{ij} = \frac{b}{4a}\begin{bmatrix} A_1 & -A_1 & -A_2 & A_2 \\ -A_1 & A_1 & A_2 & -A_2 \\ -A_2 & A_2 & A_3 & -A_3 \\ A_2 & -A_2 & -A_3 & A_3 \end{bmatrix}$$

$$BU_{ij} = \frac{a}{4b}\begin{bmatrix} B_1 & B_2 & -B_2 & -B_1 \\ B_3 & B_4 & -B_4 & -B_3 \\ -B_2 & -B_4 & B_4 & B_3 \\ -B_1 & -B_2 & B_2 & B_1 \end{bmatrix}$$

$$CU_{ij}(\phi^n) = \frac{b}{32a^2}\begin{bmatrix} C_1 & -C_1 & -C_2 & C_2 \\ -C_1 & C_1 & C_2 & -C_2 \\ -C_2 & C_2 & C_3 & -C_3 \\ C_2 & -C_2 & -C_3 & C_3 \end{bmatrix}$$

$$DU_{ij} = 8\tau \begin{bmatrix} 0 & 0 & 0 & 0 \\ 0 & 0 & 0 & 0 \\ 0 & 0 & D_1 & -D_1 \\ 0 & 0 & D_2 & -D_2 \end{bmatrix}$$

$$EU_{ij} = \frac{\phi_4^n - \phi_3^n}{2a} [DU_{ij}]$$

$$FU_i = 16\,\tau a \begin{Bmatrix} 0 \\ 0 \\ D_1 \\ D_2 \end{Bmatrix}$$

where

$$A_1 = \frac{X}{3} + \frac{Y}{4} - \frac{2W}{3} + \frac{Z}{2}$$

$$A_2 = \frac{X}{6} - \frac{W}{3}$$

$$A_3 = \frac{X}{3} - \frac{Y}{4} - \frac{2W}{3} - \frac{Z}{2}$$

$$B_1 = \frac{Y}{12} + \frac{Z}{4} + \frac{V}{4} + \frac{X}{16} + \frac{U}{8} - \frac{W}{3} + \frac{S}{2} + T$$

$$B_2 = \frac{W}{6} - \frac{Y}{12} - \frac{Z}{4} - \frac{V}{4} - \frac{X}{16} + \frac{U}{8} - \frac{S}{2} + T$$

$$B_3 = \frac{Y}{12} + \frac{Z}{4} + \frac{V}{4} - \frac{X}{16} + \frac{W}{6} - \frac{U}{8} - \frac{S}{2} + T$$

$$B_4 = \frac{X}{16} - \frac{Y}{12} - \frac{Z}{4} - \frac{V}{4} - \frac{U}{8} - \frac{W}{6} - \frac{S}{2} + T$$

$$C_1 = (\phi_1 - \phi_2)\left(\frac{Q}{4} + \frac{45R}{12}\right) + (\phi_4 - \phi_3)\left(\frac{5Q}{12} + \frac{11R}{12}\right)$$

$$C_2 = (\phi_1 - \phi_2)\left(\frac{5Q}{12} + \frac{11R}{12}\right) + (\phi_4 - \phi_3)\left(\frac{11Q}{12} + \frac{5R}{12}\right)$$

$$C_3 = (\phi_1 - \phi_2)\left(\frac{11Q}{12} - \frac{5R}{12}\right) + (\phi_4 - \phi_3)\left(\frac{45Q}{12} - \frac{R}{4}\right)$$

$$D_1 = \frac{Sa}{2} - \frac{Xa}{16} - \frac{Wa}{6} - \frac{Ua}{8} - \frac{YX_c}{12} - \frac{ZX_c}{4} - \frac{VX_c}{4} + X_cT$$

$$D_2 = \frac{Xa}{16} + \frac{Wa}{6} - \frac{Ua}{8} - \frac{YX_c}{12} - \frac{ZX_c}{4} - \frac{VX_c}{4} + \frac{Sa}{2} + X_cT$$

where

$$X = \frac{1}{P_2} - \frac{1}{P_1}$$

$$Y = \frac{1}{P_2} + \frac{1}{P_1}$$

$$W = \frac{H_2}{P_2} + \frac{H_1}{P_1}$$

$$Z = \frac{H_1}{P_1} - \frac{H_2}{P_2}$$

$$U = \frac{H_1^2}{P_1} + \frac{H_2^2}{P_2}$$

$$V = \frac{H_1^2}{P_1} - \frac{H_2^2}{P_2}$$

$$S = K_2 - K_1$$

$$T = K_2 + K_1$$

$$Q = -\frac{1}{P_1} - \frac{H_1}{P_1}$$

$$R = \frac{1}{2P_2} - \frac{H_2}{P_2}$$

which are all functions of the vertex (H_i,K_i) and the latus rectum $8P_i$ of the parabolas.

Appendix C

Elemental Equations for the Alternative Integration Method

The elemental stiffness matrix using the alternative integration method is evaluated for hyperbolic and transition elements by integrating eqs 24 over the area that influences each node. This area is the area inside the forward mach cone at position j. For example, look at the elemental stiffness matrix terms

$$K_{ij} = \begin{bmatrix} K_{11} & K_{12} & K_{13} & K_{14} \\ K_{21} & K_{22} & K_{23} & K_{24} \\ K_{31} & K_{32} & K_{33} & K_{34} \\ K_{41} & K_{42} & K_{43} & K_{44} \end{bmatrix}$$

for the bilinear rectangular element. K_{ij} is the force at i due to a unit potential at j. From this statement, the influence of each term in K_{ij} can be evaluated. For the element in Figure C-1, with mach cones shown, Figures C-2 and C-3 show which K_{ij} terms are influenced by the mach cones. Figure C-2 is for hyperbolic elements and Figure C-3 is for transition elements.

Hyperbolic Element Stiffness Matrix

The form of the stiffness matrix changes depending on whether the slope of the mach cone lines include one or two

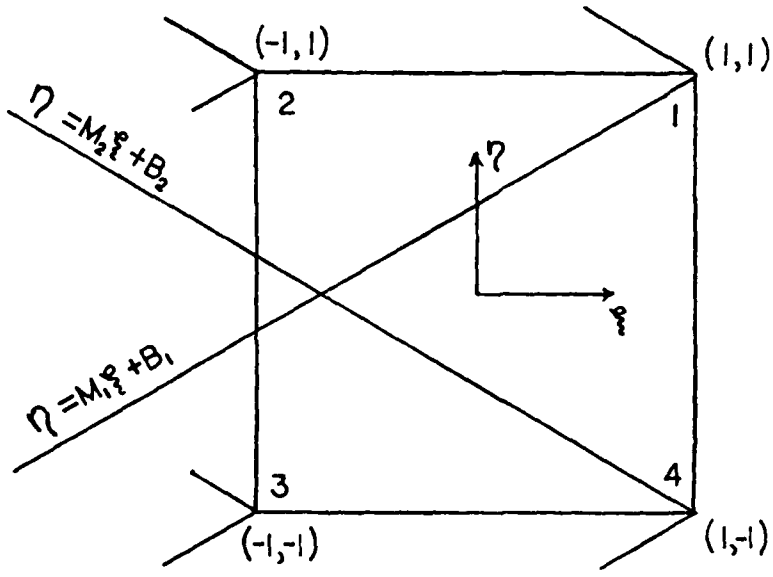

Figure C-1. Mach Cones in Hyperbolic Rectangular Element

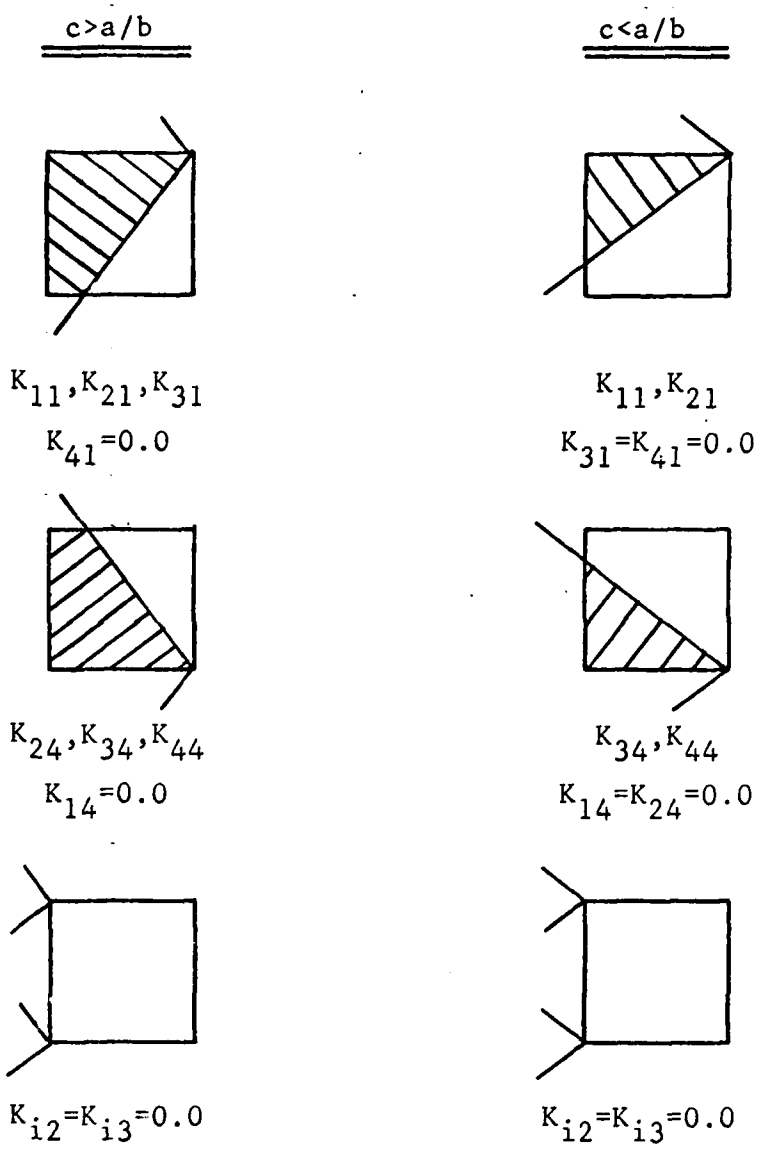

Figure C-2. Influence of Alternative Integration Method on the Elemental Stiffness Matrix for Hyperbolic Elements

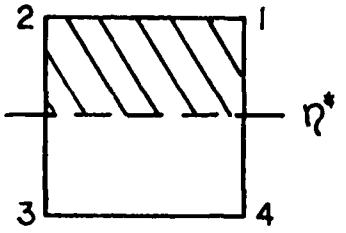

$K_{11}, K_{12}, K_{21}, K_{22}$

$K_{31}=K_{41}=K_{32}=K_{42}=0.0$

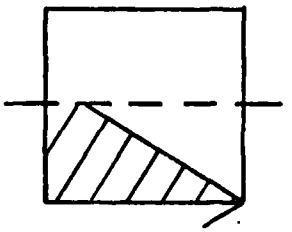

K_{34}, K_{44}

$K_{14}=K_{24}=0.0$

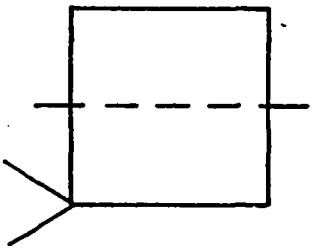

$K_{i3}=0.0$

Figure C-3. Influence of Alternative Integration Method on the Elemental Stiffness Matrix for Transition Elements

nodes (see Figure C-2). For the case where the slope c of the characteristic line is less than the aspect ratio a/b of the element, the terms of eq 23 when integrated over the area of corresponding mach cones result in

$$A_{ij} = \frac{b}{8a} \begin{bmatrix} A_{11} & 0 & 0 & 0 \\ -A_{11} & 0 & 0 & 0 \\ 0 & 0 & 0 & -A_{44} \\ 0 & 0 & 0 & A_{44} \end{bmatrix}$$

$$B_{ij} = \frac{a}{6b} \begin{bmatrix} 1-B_1-M_1 & 0 & 0 & 0 \\ \frac{1}{2}-\frac{B_1}{2} & 0 & 0 & 0 \\ 0 & 0 & 0 & \frac{1}{2}+\frac{B_2}{2} \\ 0 & 0 & 0 & -\frac{M_2}{2}+B_2+1 \end{bmatrix}$$

$$C_{ij} = \frac{b}{64a^2} \left[\begin{array}{cc} [(\phi_1-\phi_2)(C_1+C_2)+(\phi_4-\phi_3)(C_1-C_2)] & 0 \\ -C_{11} & 0 \\ 0 & 0 \\ 0 & 0 \end{array} \right]$$

$$\left[\begin{array}{cc} 0 & 0 \\ 0 & 0 \\ 0 & -C_{44} \\ 0 & \left[(\phi_1-\phi_2)(C_3+C_4)+(\phi_4-\phi_3)(C_3-C_4)\right] \end{array}\right]$$

where

$$A_{11}=\frac{7}{3}-B_1-B_1^2-\frac{1}{3}B_1^3-\frac{1}{3}M_1^2-\frac{1}{3}B_1M_1^2$$

$$A_{44}=\frac{7}{3}+B_2+B_2^2+\frac{1}{3}B_2^3-\frac{1}{3}M_2^2+\frac{1}{3}B_2M_2^2$$

$$C_1=\frac{14}{3}-2B_1-2B_1^2-\frac{2}{3}B_1^3-\frac{2}{3}M_1^2-\frac{2}{3}B_1M_1^2$$

$$C_2=\frac{17}{6}-\frac{1}{3}M_1^2-\frac{1}{10}M_1^4-B_1^2-\frac{4}{3}B_1^3-\frac{1}{2}B_1^4-\frac{4}{3}M_1^2B_1-M_1^2B_1^2$$

$$C_3=\frac{14}{3}+2B_2-2B_2^2+\frac{2}{3}M_2^2+\frac{2}{3}M_2^2B_2$$

$$C_4=-\frac{17}{6}+\frac{1}{3}M_2^2+B_2^2-\frac{4}{3}M_2^2B_2-\frac{4}{3}B_2^3+\frac{1}{10}M_2^4+B_2^2M_2^2+\frac{1}{2}B_2^4$$

B_1, B_2, M_1, M_2 FROM EQS 33

When c is greater than or equal to a/b the resulting stiffness matrix terms of eq 23 take the form

$$A_{ij} = \frac{b}{16a}\begin{bmatrix} \frac{4}{M_1}(1-\frac{2}{3}B_1) & 0 & 0 & 0 \\ -A_{11} & 0 & 0 & -\frac{4}{3}M_2(1+B_2) \\ -\frac{4}{3}M_1(1-B_1) & 0 & 0 & -A_{44} \\ 0 & 0 & 0 & \frac{4}{M_2}(\frac{2}{3}B_2+1) \end{bmatrix}$$

$$B_{ij} = \frac{a}{16b}\begin{bmatrix} G & 0 & 0 & 0 \\ H & 0 & 0 & -J \\ -H & 0 & 0 & J \\ 0 & 0 & 0 & K \end{bmatrix}$$

$$C_{ij} = \frac{b}{64a^2}\left[\begin{array}{cc|cc} \frac{1}{M_1}[(\phi_1-\phi_2)(\frac{32}{5}-4B_1)+(\phi_4-\phi_3)(\frac{8}{5}-\frac{4}{3}B_1)] & 0 & 0 & 0 \\ -C_{11} & 0 & 0 & -C_{14} \\ -\frac{1}{M_1}[(\phi_1-\phi_2)(\frac{24}{15}-\frac{4}{3}B_1)+(\phi_4-\phi_3)(\frac{16}{15}-\frac{4}{3}B_1)] & 0 & 0 & \frac{1}{M_2}[(\phi_1-\phi_2)(\frac{16}{15}+\frac{4}{3}B_2)+(\phi_4-\phi_3)(\frac{24}{15}-\frac{4}{3}B_2)] \\ 0 & 0 & -C_{41} & -C_{44} \end{array}\right]$$

where

$$G = -\frac{2B_1}{M_1} + \frac{2B_1^2}{M_1^2} - \frac{2B_1^3}{3M_1^3} + \frac{2}{3M_1^2} - \frac{2B_1}{3M_1^3} - \frac{2}{3}$$

$$H = -\frac{2B_1}{M_1} + \frac{2B_1}{3M_1^3} + \frac{2B_1^3}{3M_1^3} + \frac{2}{3}$$

$$J = \frac{2B_2}{M_2} - \frac{2B_2}{3M_2^3} - \frac{2B_2^3}{3M_2^3} + \frac{2}{3}$$

$$K = \frac{2B_2}{M_2} - \frac{2}{3M_2} - \frac{2B_2^2}{M_2^2} - \frac{2B_2}{3M_2} - \frac{2B_2^3}{3M_2^3} - \frac{2}{3}$$

In both of the above cases, D_{ij} and E_{ij} from eq 23 are the same as derived in Appendix A with $E_{33} = E_{43} = D_{33} = D_{43} = 0.0$

Transition Element Stiffness Matrix

In the transition element, the coefficient $1/c^2$ of eq 30 changes from negative to positive. A linear interpolation scheme must be employed in order to find the point η^* where the coefficient is zero. Using

$$\eta^* = 1 - \frac{2C_1}{C_1 - C_2}$$

to find this position, where C_1 and C_2 specify the value of the coefficient of eq 31 at the top and bottom of the element respectively. For terms of the stiffness matrix that deal with the mach cone from node 4, it is possible that the intercept at $\eta=-1$ be less than η^*. For this case, a new

value of intercept must be used in the limits of integration. This new term $\eta(-1)$ is calculated from the characteristic equations for $\eta=-1$. Therefore, for stiffness matrix terms that deal with the mach cone at node 4 will have an upper limit of integration given by

$$\eta^{**} = MIN(\eta^{*}, \eta(-1))$$

Now, integrating eqs 23 over the corresponding areas in Figure C-3 results in

$$A_{ij} = \frac{b}{8a} \begin{bmatrix} A_{11} & -A_{11} & 0 & 0 \\ -A_{11} & A_{11} & 0 & 0 \\ 0 & 0 & 0 & -A_{44} \\ 0 & 0 & 0 & A_{44} \end{bmatrix}$$

$$B_{ij} = \frac{a}{16b} \begin{bmatrix} \frac{8}{3} & \frac{4}{3} & 0 & 0 \\ \frac{4}{3} & \frac{8}{3} & 0 & 0 \\ 0 & 0 & 0 & B_{34} \\ 0 & 0 & 0 & B_{44} \end{bmatrix}$$

$$C_{ij} = \frac{b}{64\partial^2} \begin{bmatrix} C_{11} & C_{12} & 0 & 0 \\ -C_{12} & C_{22} & 0 & 0 \\ 0 & 0 & 0 & -C_{44} \\ 0 & 0 & 0 & C_{44} \end{bmatrix}$$

where

$$A_{11} = \frac{1}{3} - \eta^* - \eta^{*2} - \frac{1}{3}\eta^{*3}$$

$$A_{44} = \frac{1}{2M_2}\left[\frac{15}{4} + \frac{7}{3}B_2 + (B_2+1)\eta^{**} - (B_2 + \frac{3}{2})\eta^{**2} \right.$$

$$\left. + (1 + \frac{B_2}{3})\eta^{**3} - \frac{1}{4}\eta^{**4} \right]$$

$$B_{34} = \left(\frac{B_2^3}{M_2^3} + \frac{B_2}{M_2} + \frac{2}{3}\right)(\eta^{**}+1) + \left(\frac{B_2^2}{M_2^3} - \frac{1}{M_2}\right)\left(\frac{1}{2}\eta^{**2} - \frac{1}{2}\right)$$

$$- \frac{B_2}{M_2^3}\left(\frac{1}{3}\eta^{**3} + \frac{1}{3}\right) + \frac{1}{3M_2^3}\left(\frac{1}{4}\eta^{**4} - \frac{1}{4}\right)$$

$$B_{44} = \left(\frac{B_2}{M_2} + \frac{B_2^2}{M_2^2} + \frac{B_2^3}{3M_2^3} + \frac{1}{3}\right)(\eta^{**}+1) - \frac{1}{3M_2^3}\left(\frac{1}{4}\eta^{**4} - \frac{1}{4}\right)$$

$$-\left(\frac{1}{M_2} + \frac{2B_2}{M_2^2} + \frac{B_2^2}{M_2^2}\right)\left(\frac{1}{2}\eta^{**2} - \frac{1}{2}\right) + \left(\frac{1}{M_2^2} + \frac{B_2}{M_2^3}\right)\left(\frac{1}{3}\eta^{**3} + \frac{1}{3}\right)$$

$$C_{11} = 2(\phi_1 - \phi_2)\,I + 2(\phi_4 - \phi_3)\,J$$

$$C_{12} = -2(\phi_1 - \phi_2)\,J - 2(\phi_4 - \phi_3)\,L$$

$$C_{22} = 2(\phi_1 - \phi_2)K + 2(\phi_4 - \phi_3)L$$

$$C_{44} = (\phi_1 - \phi_2)\left[(B_2+1)(\eta^{**}+1) - (2+B_2)\left(\tfrac{1}{2}\eta^{**2} - \tfrac{1}{2}\right)\right.$$

$$\left. - B_2\left(\tfrac{1}{3}\eta^{**3} + \tfrac{1}{3}\right) + (2+B_2)\left(\tfrac{1}{4}\eta^{**4} - \tfrac{1}{4}\right) - \tfrac{1}{5}\left(\eta^{**5} - 1\right)\right]$$

$$+ (\phi_4 - \phi_3)\left[(B_2+1)(\eta^{**}+1) - (4+3B_2)\left(\tfrac{1}{2}\eta^{**2} - \tfrac{1}{2}\right)\right.$$

$$\left. + (6+3B_2)\left(\tfrac{1}{3}\eta^{**3} + \tfrac{1}{3}\right) - (4+B_2)\left(\tfrac{1}{4}\eta^{**4} - \tfrac{1}{4}\right) + \tfrac{1}{5}\left(\eta^{**5} + 1\right)\right]$$

$$I = \frac{15}{4} - \eta^* - \frac{3}{2}\eta^{*2} - \eta^{*3} - \frac{1}{4}\eta^{*4}$$

$$J = \frac{11}{12} - \eta^* - \frac{1}{2}\eta^{*2} + \frac{1}{3}\eta^{*3} + \frac{1}{4}\eta^{*4}$$

$$K = \frac{5}{12} - \eta^* + \frac{1}{2}\eta^{*2} + \frac{1}{3}\eta^{*3} - \frac{1}{4}\eta^{*4}$$

$$L = -\frac{13}{12} - \eta^* + \frac{3}{2}\eta^{*2} + \frac{1}{3}\eta^{*3} + \frac{1}{4}\eta^{*4}$$

The D_{ij} and E_{ij} parts of the stiffness matrix are the same as shown in Appendix B with $D_{33} = E_{33} = D_{43} = E_{43} = 0$.

VITA

Dennis L. Hunt was born on 14 January 1959 in St. Louis, Missouri. He graduated from high school in Westford, Massachusetts in 1976 and attended Embry-Riddle Aeronautical University from which he received a Bachelor of Aeronautical Engineering degree in 1980. Upon graduation, he received a commission in the USAF through the ROTC program. His first assignment was to the Air Force Institute of Technology, where he is currently pursuing a Master's degree in Aero-Mechanical Engineering.

Permanent Address: 1749 Hillside Drive
Springfield, Missouri 65804

UNCLASSIFIED

SECURITY CLASSIFICATION OF THIS PAGE (When Data Entered)

REPORT DOCUMENTATION PAGE	READ INSTRUCTIONS BEFORE COMPLETING FORM
1. REPORT NUMBER: AFIT/GAE/AA/81D-15	2. GOVT ACCESSION NO.: AD-A111 168
3. RECIPIENT'S CATALOG NUMBER:	
4. TITLE (and Subtitle): INVESTIGATION OF UPWIND SCHEMES FOR FINITE ELEMENT ANALYSIS OF TRANSONIC FLOW OVER THIN AIRFOILS	5. TYPE OF REPORT & PERIOD COVERED: MS Thesis
	6. PERFORMING ORG. REPORT NUMBER:
7. AUTHOR(s): Dennis L. Hunt, 2Lt. USAF	8. CONTRACT OR GRANT NUMBER(s):
9. PERFORMING ORGANIZATION NAME AND ADDRESS: Air Force Institute of Technology (AFIT-EN) Wright-Patterson AFB, Ohio 45433	10. PROGRAM ELEMENT, PROJECT, TASK AREA & WORK UNIT NUMBERS:
11. CONTROLLING OFFICE NAME AND ADDRESS:	12. REPORT DATE: December, 1981
	13. NUMBER OF PAGES: 92
14. MONITORING AGENCY NAME & ADDRESS (if different from Controlling Office):	15. SECURITY CLASS. (of this report): Unclassified
	15a. DECLASSIFICATION DOWNGRADING SCHEDULE:

16. DISTRIBUTION STATEMENT (of this Report)

Approved for public release; distribution unlimited

17. DISTRIBUTION STATEMENT (of the abstract entered in Block 20, if different from Report)

18. SUPPLEMENTARY NOTES

—

Approved for public release; IAW AFR 190-17

Fredric C. Lynch, Maj. USAF
Director of Public Affairs

28 JAN 1982

19. KEY WORDS (Continue on reverse side if necessary and identify by block number)

Finite Element Method
Galerkin's Method
Upwind Techniques
Mach Cones
Transonic Flow

20. ABSTRACT (Continue on reverse side if necessary and identify by block number)

Two finite element upwind techniques were investigated to see if convergent solutions could be obtained from the transonic potential equation for steady flow over thin airfoils. The first technique involves the use of parabolic upwind functions, that when added to the shape functions weight the upstream node in the supersonic region more than the downwind nodes. The second technique integrates the FE eqs over the area that influences the solution (i.e. the area inside a mach cone).

DD FORM 1 JAN 73 1473 EDITION OF 1 NOV 65 IS OBSOLETE

UNCLASSIFIED

SECURITY CLASSIFICATION OF THIS PAGE (When Data Entered)

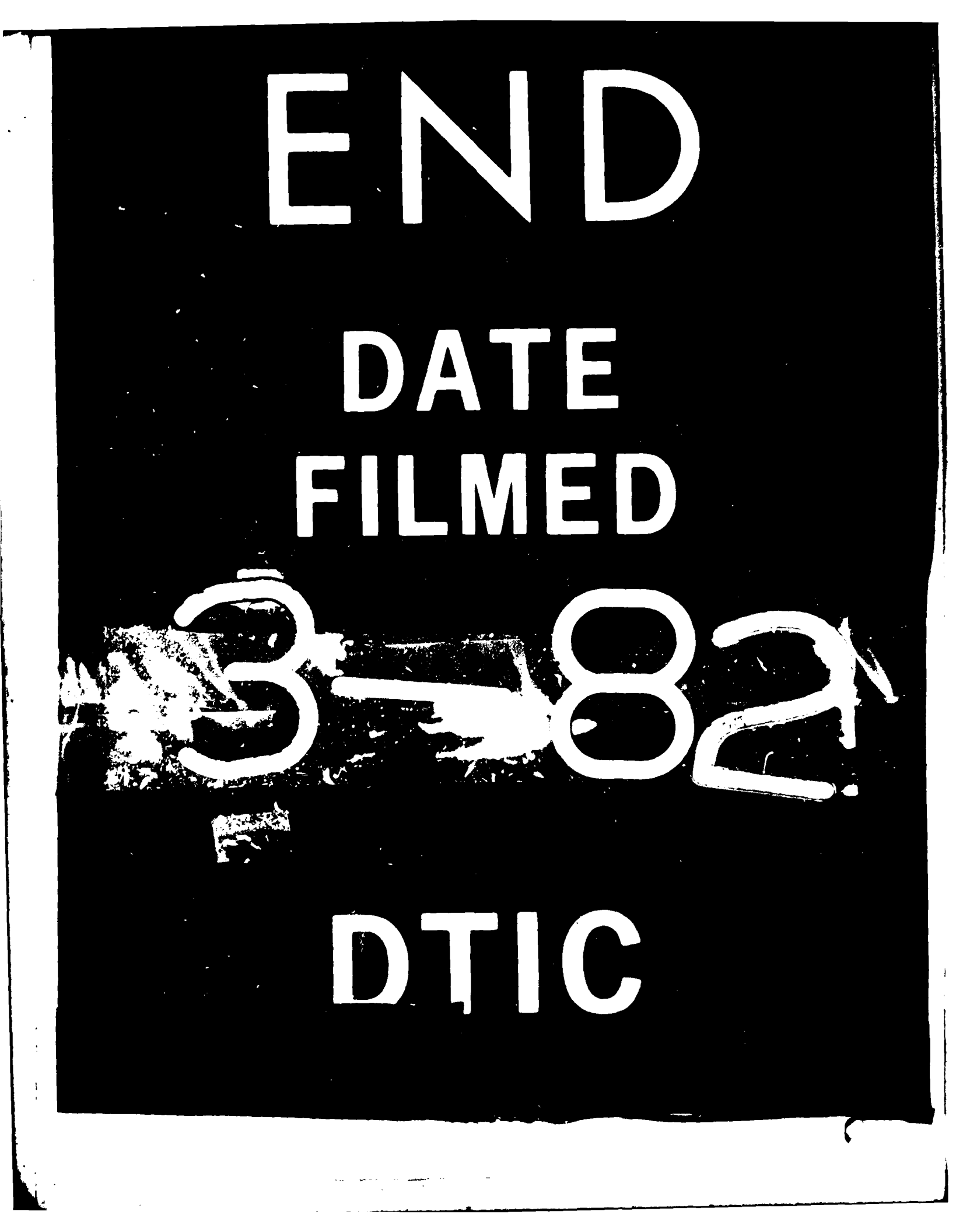
END
DATE
FILMED
3-82
DTIC